Storm-generated Holocene and historical floods in the Manawatu River, New Zealand

Ian C. FULLER[1*], Mark G. MACKLIN[1,2], Willem H.J. TOONEN[3], Katherine A. HOLT [1]

[1]Innovative River Solutions & Physical Geography Group, School of Agriculture & Environment, Massey University, Palmerston North, New Zealand

[2]School of Geography & Lincoln Centre for Water and Planetary Health, University of Lincoln, Lincoln, UK

[3]Department of Geography & Earth Science, Aberystwyth University, Aberystwyth, UK

*Corresponding author: Tel.: +64 6 356 9099; Fax: +64 350 5680; E-mail: I.C.Fuller@massey.ac.nz

Abstract

This paper reports the first reconstruction of storm-generated late Holocene and historical river floods in the North Island of New Zealand. The sedimentary infills of nine palaeochannels were studied in the lower alluvial reaches of the Manawatu River. Floods in these palaeochannels were recorded as a series of sand-rich units set within finer-grained fills. Flood chronologies were constrained using a combination of radiocarbon dating, documentary sources, geochemical markers, and palynological information. Flood units were sedimentologically and geochemically characterised using high resolution ITRAX^{TM} X-Ray Fluorescence (XRF) core scanning and laser diffraction grain-size analysis. The longest palaeoflood record extends back ca.3000 years. The temporal resolution and length of the Manawatu record reflects accommodation space for fluvial deposits, channel dynamics and mobility, and high sediment supply. Floods that occurred in the Manawatu during the mid-1800s at the time of European land clearance and in the first decade of the twentieth century appear to be among the largest recorded in the last 3000 years.

Keywords: fluvial sedimentary archive, palaeochannel, floodplain, XRF analysis

1. Introduction

Palaeoflood research in New Zealand to date has largely focused on volcanogenic break-out floods associated with the ca. A.D. 180 Taupo eruption (Manville et al., 1999, 2005), 26.5 ka Oruanui eruption from the same caldera (Manville and Wilson, 2004), and lahars generated within the Taupo Volcanic Zone (Manville, 2004; Graettinger et al*.,* 2010; Manville and Hodgson, 2011). Little attention has been given to palaeofloods beyond New Zealand's volcanic terrain, and yet storm-generated flooding is the most frequent natural hazard in New Zealand, with over 1000 serious events in the last 100 years (Willis, 2014). Assessing flood risk is, however, presently constrained by short (generally less than 60 year) gauged river flow records that poorly represent the distribution of hydrological extremes (Fuller et al., 2016). The peak discharges of early twentieth century floods have been estimated on the basis of historical records (e.g., Cowie, 1957), but human recording of floods in New Zealand is limited by its very recent colonisation, and there is a paucity of documentary evidence. Recent work using meta-analysis of a radiocarbon database developed from New Zealand Holocene alluvial records (Macklin et al., 2012; Richardson et al., 2013; Fuller et al., 2015) has produced centennial-scale records of flooding in New Zealand as a whole. While this approach has been able to identify flood-rich and flood-

poor episodes throughout the Holocene, and relate these events to broad-scale synoptic forcing (Richardson et al., 2013), it does not enable event-scale, storm-generated palaeoflood reconstruction.

Recent studies of lowland alluvial river systems have demonstrated that the grain size of individual flood beds, contained in the infill of abandoned meanders, can be used to reconstruct (palaeo)flood series (Munoz et al., 2015; Toonen et al., 2015). These records provide a tool to place recorded extreme events in a framework of long-term flooding variability. Moreover, longer flood series allow detection of distinctive phases and episodes of flooding in addition to individual events (Toonen et al., 2017), which allows comparison with other regional hydroclimatic and biological records (e.g. Norton et al., 1989; Richardson et al., 2013; Fuller et al., 2015). Furthermore, a longer flood series makes it possible to identify underlying forcing, such as El Niño Southern Oscillation (ENSO) for the Pacific region (Ely 1997; Kiem et al., 2003) including New Zealand, where the Antarctic Southern Annular Mode (SAM) is also important (Macklin et al., 2012; Richardson et al., 2013); and NAO/AMO (North Atlantic Oscillation / Atlantic Multidecadal Oscillation) for the Atlantic (Foulds and Macklin 2016; Toonen et al., 2016).

In this we paper we explore the gap in palaeoflood research in New Zealand by providing the first reconstruction of discrete storm-generated floods using analysis of the fluvial sedimentary archive, extending over the past ~3000 years. The catchment in which this work is situated lies beyond the volcanic terrain of the central North Island, removing the possibility of volcanogenic floods. The nature of topography in the Manawatu means that landslide dams in trunk rivers are rare, although significant elsewhere in New Zealand alpine terrain in association with coseismic events and/or rainfall (e.g. Korup 2002; Hancox 2005). The flood record presented here is, we believe, truly storm-generated.

2. Site description

2.1 Manawatu catchment

The Manawatu River drains a 5885 km^2 catchment situated in southern North Island of New Zealand (Fig. 1). The catchment straddles the greywacke North Island axial ranges (Tararua and Ruahine) and comprises six primary tributaries, four of which rise on the east of these ranges (Fig. 1B). The study reach, adjacent to Palmerston North, is situated in the lower part of the catchment. Mean annual discharge for the Manawatu River is ca. 110 m^3s^{-1} with the most significant contributions derived from the upper Manawatu (ca. 27 m^3s^{-1}), Mangatainoka (ca. 18 m^3s^{-1}), Pohangina (ca. 17 m^3s^{-1}), Tiraumea (ca. 16 m^3s^{-1}), Mangahao (ca. 15 m^3s^{-1}), and Oroua (ca. 13 m^3s^{-1}) (figures derived from Henderson and Diettrich 2007). The catchment was extensively cleared of native forest in a period spanning the late 1800s and early 1900s to make way for mostly pastoral agriculture (Fig. 1C). Native forest remains on

the greywacke ranges, which rise to 1695 m and 1505 m in the northernmost and southernmost parts of the catchment respectively. The Manawatu River crosses the axial range through the Manawatu Gorge, which is the only locality for significant dambreak floods in the trunk river and primary tributaries. However, the evidence is not clear (geological, documentary, or Maori oral tradition) of the river having been completely dammed by landslides here in the late Holocene, although the presence of large boulders in the channel floor of the Gorge indicates significant local, off-slope delivery. With the exception of the uplifted greywacke fault block, most of the catchment is underlain by soft sedimentary rock, notably mudstones and sandstones (Fig. 1D). Erosion of this terrain generates a suspended sediment yield from the Manawatu to the ocean of ca. 3.74 Mt y^{-1} (Hicks et al., 2011). While this volume of sediment discharge has no doubt been enhanced by land clearance (Hicks et al., 2011), the underlying soft-rock terrain is likely a naturally high sediment generator. Clement et al. (2017) recorded a rapid infilling of the Manawatu estuary within ca. 2700 years of the mid-Holocene sea level high-stand (7240-6500 cal. YBP). Tectonic uplift in the catchment is ca. 1-4 mm y^{-1} in the greywacke ranges (Wellman, 1972; Pillans, 1986; Whitehouse and Pearce, 1992), and river terraces generated by downcutting in response to this uplift are prominent landscape features in the upper and middle reaches of the primary valleys.

Figure 1.

2.2 Climate

Climate in the region is humid temperate; mean annual rainfall in Palmerston North is ~980 mm, rising to >2000 mm in the Tararua and Ruahine ranges (NIWA 2017). Most rain in the catchment is brought by mid-latitude frontal systems approaching from the west, although subtropical depressions in late summer-autumn and southerly polar outbreaks (throughout the year) can bring easterly-quarter rain. Temperatures are mild: the mean temperature in the coldest month (July) is 8°C, rising to 18°C in the warmest month (February). Snow at sea level is extremely rare (~30-year recurrence interval), although snowpacks above the tree line (~1000 m) can develop during sustained cold periods.

2.3 Floodplain topography

In the lower Manawatu valley in the vicinity of Palmerston North, the valley floor widens and becomes unconfined as the river emerges into the Taonui basin (cf. Fig. 2). Here, a sequence of palaeochannels, abandoned by natural neck and chute cutoffs, has been well preserved on the floodplain (Fig. 2).

Upstream of Palmerston North, the floodplain is bound by early Holocene and late Pleistocene river terraces, while a last interglacial marine terrace forms a higher (100 m) surface to the south of the floodplain (cf. Fig. 2 and Clement et al. 2010). River management has straightened the channel through much of this reach (Page and Heerdegen 1985), and the river is now largely disconnected from its floodplain by the Lower Manawatu Flood Protection Scheme, providing flood protection for the city of Palmerston North and for the high value dairy agriculture of the lower valley. The river gradient flattens significantly within this reach from 0.0012 upstream of the city to 0.0002 downstream of the 10-m contour (Fig. 2) (Page and Heerdegen 1985). The sequence of palaeochannels in the lower Manawatu was first described by Page and Heerdegen (1985), noting that they were already defunct at the time of a previous survey in 1859. Page and Heerdegen (1985) describe partial infilling of these palaeochannels with up to 8 m of fine-grained sediments overlaying gravels of the original channel bed, and their interpretation suggested that some of these channels were abandoned around 200 years prior to the 1859 survey because the depth of soil formation and amount of infilling, which was only a little greater than that of other dated cutoffs (1888 and 1937). If that interpretation was correct, these palaeochannels would yield records of past floods spanning ~350 years. However, we should also note that Page and Heerdegen's mapping of the palaeochannel sequence is somewhat incomplete. Terrain surfaces generated from airborne LiDAR acquired by the Horizons Regional Council in 2006 have revealed several more distal and evidently older palaeochannels in the Manawatu. The full suite of palaeochannels is described by LoRe et al. (2018).

Figure 2.

3. Methods and Data

Cores of selected palaeochannels were recovered using a hydraulic percussion coring system in distal palaeochannels containing consolidated sequences and a Livingston piston corer in wetter palaeochannels with a soft sediment fill proximal to the current river. Cores were split, with one-half being shipped for ITRAX™ X-Ray Fluorescence (XRF) core scanning and grain-size analysis at Aberystwyth University (UK), while the remainder was sampled for palynological analysis and radiocarbon dating.

3.1 Grain-size analysis and identification of flood units

Flood units are identifiable as sandy layers in the silt-dominated cores (see Figs 6 and 7). A Malvern 2000 laser diffraction device was used to measure grain-size distribution of 1-cm-thick samples, taken at 5-10 cm intervals. Samples were pretreated with $Na_4P_2O_7.10H_2O$ and sonic disaggregation to disperse grains in order to prevent flocculation. In total, 402 samples were collected from the cores. Previous studies indicate that grain-size information of flood deposits can relate to flood magnitudes (Jones et al., 2012; Munoz et al., 2015; Toonen et al., 2015; Leigh, 2017). However, continuous study of flood laminae at a high-resolution (mm scale) is inefficient and costly. Jones et al. (2012) demonstrated that the Zr/Rb ratio provides a robust geochemical proxy for the grain size of flood deposits in low-gradient Welsh river systems. The element Zr is found principally in the resistant mineral zircon, while Rb is found in a range of minerals including clay minerals. Zirconium tends to become concentrated in fine sand to coarse silt, while Rb concentrates in fine silt and clay during sediment transport, which means an increasing Zr/Rb ratio can be associated with an increase in grain size (Jones et al., 2012). The ITRAX™ XRF core scanning was used to measure core geochemistry at a 1-mm resolution.

To test the relation between direct measurement of grain size using laser diffraction and the Zr/Rb geochemical proxy grain size, sampling targeted (i) visually recognisable coarse-grained flood layers and fine-grained background sedimentation (originating from more common events) and (ii) specific intervals of high or low (peak and troughs) Zr/Rb ratios. This approach ensures that the Zr/Rb grain-size proxy is validated for the full range of sediments that occurs in the channel fill sequences.

The Zr/Rb count ratio was normalised for each single measurement using the sum of coherent and incoherent scatter (dependent upon organic and water content). Measurements were averaged over an 11-mm interval to fit with the sample size used for laser diffraction grain-size analysis. A comparison was made with the D_{50} and D_{90} parameters (Fig. 3A). The data are presented as a bulk ensemble for all sites because all sites are located in the same river reach and share a common stratigraphy, lithology, and catchment. The relation between D_{50} and D_{90} appears consistent between all sites and is significant (n = 400, r = 0.89, $p < 0.001$), cf. Fig. 3. A statistically significant relationship exists between the grain size and the Zr/Rb ratio: D_{50} vs. Zr/Rb ($r = 0.68$, $p < 0.001$; Fig. 3B) and D_{90} vs. Zr/Rb ($r = 0.49$, $p < 0.001$). Both correlations are significant at n = 360 (excluding the grain-size samples that do not overlap with geochemistry measurements e.g. near gaps and sections unsuitable for scanning). However, the Zr/Rb ratio is more strongly correlated with the D_{50} than the D_{90}. A divergence in the relationship between grain size and Zr/Rb ratio occurs above ~0.8, and this corresponds to the greater proportion of medium sand deposited before the cutoffs were finally separated from the main flow (Fig. 3B). Because the D_{50}/D_{90} ratio is stable and significant, we can infer the use of D_{50} would equally

represent flood magnitude variability as well as of D_{90} at these sites. This test thus confirms that peaks in the Zr/Rb ratio correspond with flood units and that the Zr/Rb ratio provides a robust grain-size proxy (Turner et al., 2015). The ITRAX™ XRF core scanning, calibrated on laser diffraction grain-size samples, was thus deployed as a grain-size proxy to provide a detailed flood sedimentology from the Manawatu cores.

General trends in grain size may result from changes in proximity to the river channel or the progressive buildup of levees, limiting sediment dispersion across the floodplain (Toonen et al., 2015; Leigh, 2017). Following Jones et al. (2012), in order to account for these geomorphological effects, a 10-cm running filter was used to detrend the data. The detrended data were converted into *Z*-scores to present alongside the Zr/Rb ratio to identify flood units in the cores.

Figure 3.

As part of ITRAX™ XRF core scanning, contaminant metal levels were also measured. These show consistent trends, and Cu and Zn can be used to identify twentieth century floodplain contamination associated with urban and industrial growth (Appendix).

3.2 Documented historical and late Holocene floods

Flood chronologies were constrained using a combination of instrumental flow records, documentary sources, and geochemical markers associated with pollution, palynology, and radiocarbon dating. Exploratory use of ^{210}Pb and ^{137}Cs was deployed on the Hamilton 1 core in order to better constrain the timing of floods recorded in this sedimentary archive with gauged floods. Channel cutoff of Hamilton 1 occurred in A.D. 1937. Figure 4 provides a record of the largest gauged and documented floods in the Manawatu River in each year, as measured at the gauging station in Palmerston North. The Manawatu River has the longest continuous gauging record in New Zealand, extending to 1923, with estimates of flows prior to this made with reference to observation of river levels (Page, 1994). Figure 4 is a synthesised flow record from observations and gauged data that were measured at three sites in close proximity (Fitzherbert 1923-1971, Ruahine Street 1971-1987, and Teachers College 1987-present). The three gauging sites can be regarded as a continuous series (Henderson and Diettrich 2007). Flood depths at each palaeochannel have been modelled by Horizons Regional Council (Table 1; J. Bell, pers. comm. 2017). Although not modelled, a flow of 4512 m^3s^{-1} is estimated to have an

annual recurrence interval (ARI) of 500 years, and a flow of 5345 m^3s^{-1} is estimated to have an ARI of 2500 years at Teachers College (J. Bell pers. comm. 2017). The modelled ARI of flood depths at each site was used to infer the minimum flood magnitudes needed to produce flood units for each individual sites. Estimation of sediment accumulation rates was feasible where cutoff dates were known or reasonably well constrained by indirect dating (^{14}C and palynology; see below).

Figure 4.

Table 1

Modelled flood depths for given flood ARIs and magnitudes at each palaeochannel site, in a synthetic situation without stopbanks (flood embankments) but using the current topography; flood magnitudes and return periods were calculated at Teachers College (J. Bell, pers. comm. 2017)

		Approx. modelled depth of flooding (m)				
	ARI (y):	1	2	10	50	100
Palaeochannel	Q (m^3 s^{-1}):	507	1488	2462	3317	3678
Hamilton 1		0.5	3	3	3.5	4
Karere 2		nf	2	2	3	3.5
Palmy Park		nf	nf	1	2	3.5
Riverside Drive		nf	nf	1	1.5	2
Hamilton 2		nf	1	1	1.5	2
Alpaca		nf	2	2	3	3.5
Opiki		nf	nf	2.5	3	3.5
Rocket		nf	1	1.5	2.5	3
Napier Rd		nf	nf	1	1.5	2.5

nf: not flooded.

The largest documented flood in 1857 was estimated to have a peak discharge of 4010 m^3 s^{-1} (Page, 1994). Observations indicate that this flood was generated by an extensive whole-catchment rain event (Page, 1994), possibly in early December, based on a newspaper report of severe flooding in the Turakina catchment ~20 km to the northwest of the Manawatu watershed (*Wellington Independent*, 9 December 1857), but no definitive date is available. Six additional floods exceeding 3000 m^3s^{-1} have been documented since 1857, these occurred in March 1880, April 1897, June 1902, July 1906, January 1953, and February 2004, indicating that large floods are not related to any particular season.

3.3 Linking documented floods with the sedimentary record

Documented floods were linked to the flood sedimentary record by first determining date of cutoff, which provides a secure age for the onset of flood sedimentation in the abandoned channel. At Hamilton 1 exploratory ^{210}Pb and ^{137}Cs analysis was used to identify peak deposition of ^{137}Cs at ca. 1965, with no deposition prior to 1952. Ten-gram samples were taken at 10-cm intervals downcore and indicate that at least the upper 3.0 m of sediment was deposited post-1952 (Table 2). Analysis was undertaken under contract by the Institute of Environmental Science and Research Ltd, Christchurch. Samples were counted on HPGe (high-purity germanium) detectors with counting time ranging from 48 to 68 hours. For those palaeochannels beyond the stopbanks (embankments providing flood protection) on the inactive floodplain, the last recorded flood is generally 1953. Inferred ages of flood units observed in the cores can reasonably be inferred by comparison with the documented record, taking into account the likelihood of sufficient inundation (cf. Table 1) for the given flood magnitude. Effectively a counting down from the top of the core, and/or up from known date of cutoff, provides a means of assigning flood units to specific documented flood events. This was most straightforward for the few largest events, which were presumed to match rarely occurring coarse flood units. Elevated concentrations of heavy metals in palaeochannel cores reflect pollution associated with the urban growth of Palmerston North from the early twentieth century. Pollen evidence and radiocarbon dating were also used to secure age control.

Table 2

Radioactive isotope analysis, Hamilton 1 core

Sample number	Client code	Lead-210 (Bq/kg)	Caesium-137 (Bq/kg)	Radium-226 (Bq/kg)	Radium-228 (Bq/kg)
2017-1539	H1 0.1 m	4.1 ± 9.7	< 0.86	32.5 ± 2.5	40.2 ± 3.7
2017-1540	H1 0.2 m	32.2 ± 6.2	0.65 ± 0.25	35.3 ± 2.9	44.5 ± 3.5
2017-1541	H1 0.3 m	37.7 ± 9.4	< 0.88	35.6 ± 2.8	44.1 ± 4.0
2017-1542	H1 0.4 m	32.1 ± 3.7	0.48 ± 0.27	42.9 ± 8.3	53.0 ± 1.4
2017-1543	H1 0.5 m	47 ± 11	< 1.3	40.1 ± 2.9	48.8 ± 4.0
2017-1544	H1 0.6 m	47 ± 14	< 1.5	36.2 ± 3.2	41.8 ± 4.6
2017-1545	H1 0.7 m	23.2 ± 5.3	0.76 ± 0.40	41.4 ± 2.8	47.4 ±3.7
2017-1547	H1 0.9 m	39 ± 11	1.0 ± 0.53	35.8 ± 3.6	43.5 ± 4.6
2017-1549	H1 1.1 m	48.6 ± 7.5	<1.6	36.7 ± 4.2	48.2 ± 5.6
2017-1551	H1 1.3 m	35.4 ± 5.5	0.66 ± 0.47	37.4 ± 3.6	48.2 ±4.7
2017-1553	H1 1.5 m	39.7 ± 7.1	<1.9	40.5 ± 3.7	52.7 ± 5.9
2017-1555	H1 1.7 m	38 ± 11	< 1.7	40.9 ± 3.2	48.5 ± 4.4

2017-1557	H1 1.9 m	31.2 ± 5.9	< 1.6	35.5 ± 3.1	42.2 ± 4.7
2017-1559	H1 2.1 m	43.7 ± 6.4	1.67 ± 0.56	44.0 ± 1.3	50.6 ± 2.3
2017-1561	H1 2.3 m	39.0 ± 8.3	1.95 ± 0.73	52.1 ± 3.8	61.5 ± 5.2
2017-1563	H1 2.5 m	39.5 ± 6.0	1.56 ± 0.61	43.3 ± 3.3	52.9 ± 4.5
2017-1565	H1 2.7 m	39.1 ± 6.2	1.40 ± 0.52	45.9 ± 1.3	53.5 ± 2.3
2017-1567	H1 2.9 m	47.6 ± 7.5	1.90 ± 0.76	49.4 ± 3.8	65.7 ± 5.6
2017-1569	H1 3.1 m	37.4 ± 8.1	1.06 ± 0.64	44.5 ± 3.4	55.0 ± 4.8
2017-1571	H1 3.3 m	32.2 ± 6.6	<1.3	37.1 ± 2.6	45.3 ± 3.8
2017-1573	H1 3.5 m	47.7 ± 7.9	<2.2	41.3 ± 4	54.6 ± 5.3
2017-1575	H1 3.7 m	43.6 ± 7.7	<2.0	39.2 ± 4.2	50.9 ± 5.8
2017-1577	H1 3.9 m	40.5 ± 7.6	<2.0	42.4 ± 3.7	50.1 ± 6.2

3.4 Palynology

Sediments from fluvial depositional settings are seldom selected for use as palaeovegetation archives given the potential for reworking, the episodic nature of deposition, and the typically large pollen source area. Thus, they are generally of little value for providing detailed reconstructions of local-scale vegetation and climate change. However, they can still provide qualitative indications of broad scale changes in the vegetation of the catchment, such as evidence for periods of major vegetation clearance and the introduction of exotic species, both of which are driven by human activities. Because the timing of Polynesian and European colonisations in New Zealand are well constrained, pollen indicators of these events can therefore provide a rough chronology for deposits in which they occur.

Samples for pollen analysis were taken from unoxidised sediments from cores from five of the study sites, as oxidation in the remainder precluded pollen preservation. For all cores, this excluded the upper 50-100 cm approximately. Samples were processed according to the standard methodology documented in Moore et al. (1991), with residue mounted in silicone oil and examined at 400x magnification under a Zeiss Axiophot microscope.

In New Zealand pollen records, Polynesian and European phases of colonisation are represented by distinctive signals (e.g. Wilmshurst, 1997; McGlone and Wilmshurst, 1999). Polynesian arrival is marked by a decline in native forest pollen and concurrent rise in successional species. European colonisation is marked by further decline in native forest pollen, and the appearance of exotic species introduced for agricultural and horticultural purposes.

We have used the appearance of key exotic taxa (e.g. *Pinus radiata*, *Salix*, *Taraxacum*, etc.) as indicators of the presence of Europeans somewhere within the catchment, thus providing some basic

chronological control. No definitive signals of deforestation and subsequent succession from either Polynesian or European activities were discernible in the records obtained in this study. This probably reflects muting of the signals of clearance of individual catchments by the continued input of forest pollen from the subcatchments that remain forested.

Summary pollen diagrams for the five sites where pollen was analysed are shown in Fig. 5. As a proof of concept, we chose to investigate Hamilton 1 for pollen, as it provides a benchmark for what we can expect a post-colonisation pollen signal to look like within flood sediments. Pollen of native trees and shrubs are the dominant pollen types recorded despite much of the native forest being cleared during the timespan covered by the Hamilton 1 site. This probably reflects the relatively high pollen production and also the robustness of the pollen grains of some canopy-forming trees present in the remaining native forest in the catchment headwaters. Pollen of introduced pasture herbs (*Plantago lanceolata* type, *Rumex*, and *Taraxacum*) are present in low levels, but consistently so. Pine pollen appears in the middle of the sequence, becoming more abundant towards the top, probably representing the expansion of *Pinus radiata* forestry in the mid-late twentieth century. Thus, the Hamilton 1 data indicate that a European pollen signal is persevered within these fluvial sediments, but it is considerably more subtle than the signals seen in lake and bog sequences that are only capturing pollen from the immediate vicinity of the site.

Figure 5

3.5 Radiocarbon dating

Table 3 provides details of the radiocarbon dates. Ages were calibrated using OxCal version 4.3.2 (Bronk Ramsey et al., 2017) and the SHCal 13 atmospheric curve (Hogg et al., 2013). Obtaining enough organic matter for radiocarbon dating from these cores was challenging. While most cores contained scattered macroscopic fragments, these were seldom in sufficient concentration to yield enough material for an AMS radiocarbon date. To try to resolve this issue, organic matter from bulk sediment samples from Rocket and Opiki cores was concentrated by removing the clastic matter with hydrofluoric acid. Samples from the Rocket core with 0.85 m between them were not distinguishable by age. This could reflect inclusion of reworked organic matter in the samples, suggesting bulk concentration is not a viable method. However, it may also simply reflect rapid infilling of the channel. The pollen data from the Rocket core suggest that the entire core accumulated prior to the arrival of humans, which is consistent with the radiocarbon age. However, the Opiki sample was collected from

289 ca. 0.3 m below where we encounter pollen signals of European presence, so an age of 1722 cal. YBP
290 seems an overestimation. This could also be the result of older organic matter in the dated sample or
291 perhaps a hiatus in sedimentation. The Napier Road sample comprised macroremains (leaves, twigs,
292 etc.) and can be considered more reliable, and ^{14}C ages are consistent with the pollen data.

293

294 **Table 3**

295 Radiocarbon dates

Site	Sample ID	Lab code	Sample material	Depth (m)	^{14}C AMS	Calibrated age (years)
Napier Rd	Napier Road	WK-43116	Leaves and twigs	2.27-2.31	2009 ± 20 BP	2050-1926 cal BP
Rocket	Rocket OC1	WK-43117	Bulk organics	3.85-3.90	2663 ± 20 BP	2831-2775 cal BP
	Rocket OC2	WK-43118	Bulk organics	2.99-3.04	2696 ± 20 BP	2850-2792 cal BP
Opiki	Opiki	WK-43119	Bulk organics	2.50-2.54	1722 ± 20 BP	1745-1585 cal BP

296

297

298 **4. Results and Interpretation**

299 Of the nine cores extracted from the Manawatu palaeochannels, four were located on the current
300 floodplain (Fig. 6; Appendix: Figs. A1-4). The remaining five sites were located beyond stopbanks in
301 the protected floodplain (Fig. 7; Appendix: Figs. A5-9), which no longer has flood-related
302 sedimentation. Stopbanks in the Lower Manawatu Flood Protection Scheme are rated as providing
303 '500-year' flood protection (Watson, pers. comm., 2017). A schematic (Fig. 8) summarises the results
304 from the cores described in detail in this section and displays their relative position on the floodplain.

305 The observed flow record of the Manawatu (Fig. 4) has been mapped to each major flood event
306 detected using the Zr/Rb ratio and *Z*-score, taking into account the age of the palaeochannel and
307 available chronology in the core (pollen, radiocarbon ages, and historical information). Based on the
308 modelled flow depths (Table 1), floods with magnitudes around and >2000 m^3s^{-1} will potentially leave
309 a sediment signature at all sites (cf. Table 1). Smaller floods will also inundate the more proximal
310 channels. Hamilton 1 and Karere 2 (Fig. 6; Figs. A1-2) are located within the Manawatu stopbanks and
311 potentially provide a record of every flood since stopbank construction in the early 1960s; however,

312 the upper metre of these cores was not scannable (too brittle with heavy bioturbation and oxidation),
313 and the past ca. 20 years of record is missing (Fig. 8).

314

315

316 **Figure 6.**

317 **Figure 7.**

318 **Figure 8.**

319

320 *4.1 Active floodplain sites*

321 Hamilton 1, Karere 2, Riverside Drive, and Napier Road cores are located in the currently active
322 floodplain. Full results are presented in the Appendix. Figures 6 and 8 summarise the floods inferred
323 from *Z*-score results (Appendix) and correlates these to the documented flood record. Results for
324 Hamilton 1, Riverside Drive, and Napier Road are described in detail below (see also Fig. 8). Karere 2
325 is described in the Appendix as it is very similar to Hamilton 1, being an historical cutoff from 1888
326 (Page and Heerdegen, 1985).

327

328 *4.1.1 Hamilton 1*

329 The oldest flood in Hamilton 1 dates to 1937, when this bend was abandoned (Page and Heerdegen,
330 1985), and cutoff was coincident with a flood >2000 $m^3 s^{-1}$ (cf. Fig. 6). The site was flooded recently in
331 2015 and 2004. The coarser and deeper part of the palaeochannel sequence probably accumulated
332 rapidly, when an open connection with the active channel existed (cf. Toonen et al., 2012), potentially
333 including the years before a full cutoff was established. Within-channel sediments in the lower part of
334 the core demonstrate an open connection with the active channel for some short, but unknown,
335 period. During this period coarse sediment could be conveyed into the abandoning channel. This did
336 not necessarily occur during the earliest annual maximum peak discharges of 1941 and 1942 but could
337 equally have occurred during higher flows throughout the year because of (periodic) connection with
338 the channel, allowing rapid deposition to take place. Because of this connection, 35 cm of
339 sedimentation during a single year or flood in this depositional context is not unusual. At the time
340 when the channel was fully disconnected (1953 and 1956), variability in grain size and sedimentation

rates has to be related to sediment deposited by overbank floods or to pulses of sedimentation during a single large event (cf. Macklin et al., 1992). Annual peak floods may all have been preserved in the period directly following the initial abandonment in 1937, as all inundated this site (cf. Table 1). Therefore, the flood unit at 4.33 m matches with the 1941 flood, which also exceeded 2000 $m^3 s^{-1}$. Average sedimentation rate since abandonment is 58 mm/y, 455 cm between A.D. 2015 and 1937, with higher rates near the bottom and toward the top of the sequence based on general trends in channel fill grain sizes and ^{137}Cs data (cf. Table 2). Therefore, the missing scanned section in the upper part of the core is estimated to represent at least ~25 years. Hence, recent large events (e.g. 3500 m^3s^{-1} flood in February 2004 and 2500 m^3s^{-1} flood in July 1992) are not present in the record. Floods exceeding 2500 m^3s^{-1} occurred in May 1941, January 1953, July 1956, and March 1965, which according to Table 1 would inundate the site to a depth of 3 m. An initial chronology is provided in Fig. 6. The coarse-grained part of the sequence has probably accumulated during the initial flood events after abandonment and the majority with the large 1941 flood (2605 m^3s^{-1}). After ca. 1941, the channel became less connected from the main river, resulting in dramatic reduction of channel fill grain size. If the larger peaks (>2.5σ) relate to floods with a discharge >2000 m^3s^{-1}, then the latest flood to be recorded locally would be the October 1988 event. This fits the previous assumption that at least the last 25 years was missing. The large March 1965 (2744 m^3s^{-1}) and January 1953 (3176 m^3s^{-1}) events are presumably also registered as peaks in grain-size proxy (*Z*-score). Based on the inferred ages at 1 and 4 m, respectively 1980s and 1940s, these events should be present in the central part of the core. The two largest peaks in grain size can be found between 2 and 3 m depth. Despite the greater peak discharge of the 1953 event, the *Z*-score is slightly smaller than the 1965 flood. The grain size of flood deposits is dependent on the shape of the hydrograph and on hysteresis effects on river sediment load, not simply related to flood magnitude. Peaks in grain size tentatively match with peak flows exceeding 2000 m^3s^{-1} (Fig. 6). Smaller peaks were left unassigned because at this site these can relate to any discharge exceeding just 500 $m^3 s^{-1}$ (Table 1) and because these relatively minor annual peak discharges or second-ranked annual events are not considered in this study.

4.1.2 Riverside Drive

Riverside Drive (Figs. 6, A3) was abandoned before 1859 (inferred from position of the river surveyed in 1859; Manawatu Catchment Board, 1982) and last inundated in 2004 (personal observation, ICF). This site is located in an area of floodplain without stopbanks and is confined by high fluvial terraces (cf. Fig. 2). The 2004 flood is likely the *Z*-score peak in the upper 0.2 m. The entire core consists of an overbank sequence without major changes in grain size (below 1 m, deposits are a little coarser, probably reflecting proximity to the active channel). High Zn and Cu in the upper 5 cm are associated

with modern pollution (Fig. A3). Several other distinct high peaks of Zn are located in the upper metre, and a single high peak of Pb was measured around 75 cm. These might be related to specific pollution-spillage events that must have occurred after the 1880s when industrialisation of the region commenced (Manawatu Catchment Board, 1982). If the 2004 event (3515 $m^3 s^{-1}$) is related to a Zr/Rb *Z*-score of >2σ, previous events of a similar *Z*-score are likely associated with events exceeding 3000 $m^3 s^{-1}$ as well. Based on this assumption, peaks can be correlated with the large floods of January 1953 (3176 m^3s^{-1}), the events of May 1907 (3340 m^3s^{-1}), June 1902 (3800 m^3s^{-1}), and April 1897 (3333 m^3s^{-1}), which form a cluster of large floods at the turn of the twentieth century, and March 1880 (3980 m^3s^{-1}). The position of the 1880 event is consistent with an increase in contaminant metal concentrations associated with early industrialisation and urbanisation in the Manawatu catchment. Before 1880 the discharge record is incomplete and the correlation becomes more tentative. However, the 1857 event (4010 m^3s^{-1}) is the largest event recorded and is likely associated with the coarsest flood units at c. 1.5 m depth. If the same accumulation rates apply for the deeper part of the core, this flood record goes back to the early nineteenth century and contains several historically unknown floods of large magnitudes (in the realm of 3000-4000 m^3s^{-1}).

4.1.3 Napier Road

Napier Road (Figs. 6, A4) is the most distal palaeochannel in the upper part of the study reach, adjacent to the Late Pleistocene river terrace. It was abandoned at an indeterminate pre-1859 date (inferred from river position in 1859; Manawatu Catchment Board, 1982), and a radiocarbon age of 2050-1926 cal. BP at 2.27-2.31 m (Table 2) suggests a likely 2-3 ka record of flooding at this site. Pollen of European introduced herbs (specifically *Plantago* and *Taraxacum*) dating to ca. A.D. 1840 appears between 161 and 156 cm depth within the Napier Road core. Radiata pine (*Pinus radiata*) is first recorded at c. 75 cm depth, representing the expansion of pine forestry in New Zealand in the mid-twentieth Century. In more recent flood events, although not stopbanked, the site is probably disconnected from floods by a main (elevated) road, so the 1953 (3176 m^3s^{-1}) flood is likely the most recent to inundate the site (no river flooding in 2004). The lower part of the core is relatively coarse with many flood units, the middle section (60-200 cm) is silty with several thick flood units in the top, and the upper 60 cm is very fine organic clay, commensurate with a disconnection from river floods, and likely reflects ponding from local surface and stormwater runoff. The units between 60 and 100 cm represent large floods and probably relate to the cluster of floods at the turn of the twentieth century. This is consistent with elevated Zn concentrations in these units (Fig. A4).

Older (>2050-1926 cal. BP) coarse deposits toward the base of the Napier Road core are likely to reflect channel proximity at this time, rather than indicating large floods analogous to the situation

described at Hamilton 1. However, a period of significantly enhanced river activity recorded in the North Island from ca. 2400-2100 cal. BP (Fuller et al., 2015), suggests that large floods (ca. >3000 m^3 s^{-1}) may have occurred during this period. Importantly, the evidence from the Napier Road core is consistent with the meta-analysis of Fuller et al., (2015).

4.2 Inactive floodplain sites

Palmy Park, Hamilton 2, Alpaca, Opiki, and Rocket are located beyond stopbanks on the protected floodplain; they are no longer affected by current overbank sedimentation. Full results are presented in the Appendix (Figs A5-9). Figure 7 summarises the floods inferred from the *Z*-score results (Appendix) and correlates these to the documented flood record. Results for Palmy Park, Hamilton 2, and Rocket are described in detail below. Alpaca is described in the Appendix for the sake of brevity.

4.2.1 Palmy Park

Palmy Park (Figs. 7, A5) records Manawatu floods between the 1960s and at some point prior to 1859 (inferred from river position in 1859; Manawatu Catchment Board, 1982); however, following 1960s stopbank construction, inundation still occurred associated with overspill from the Mangaone tributary that flows within the western limb of this palaeochannel. Pollen data indicate European impact starts between 100 and 132 cm, ca. A.D. 1840. The upper section was too brittle for ITRAX™ scanning and heavily bioturbated. At 130 cm a very clear and rapid transition from sandy material to overbank clays is observed. Few flood units are visible, but those present are very clear with thick units, reflected in the *Z*-score plots. High peaks of Zn and Pb occur around 1 m, and in the upper metre a clear trend of increasing contaminant metal concentration (Zn, Ni, Cu, Pb) is visible. The earlier peaks probably relate to the onset of industrialisation in the late nineteenth century, while the general increase is later (probably mid-twentieth century related to the expansion of Palmerston North). The large events clustered between 100 and 120 cm can be matched with large floods at the turn of the twentieth century (i.e., 1907, 1902 and 1897). Events predating this period have produced significantly larger peaks in the *Z*-score proxy grain-size record-notably around 130 cm and below 160 cm. Based on the palynological information and historical maps (abandonment of the channel before 1859), these peaks likely relate to extreme floods that occurred in the nineteenth century, probably those of 1880 and 1857. Several other large floods can be observed in the record before the flood-intense episode centred on the ~1850s.

4.2.2 Hamilton 2

Hamilton 2 (Figs. 7, A6) is located beyond stopbanks and away from tributary influences. The channel was abandoned (shortly) before 1859 (inferred from river position in 1859; Manawatu Catchment Board, 1982), and the last inundation was the 1953 flood prior to stopbank construction. Several clear trends were visible in channel-fill sedimentology. First, at the bottom a stepwise abandonment of the site with progressively finer overbank deposits is evident. Around 2.50 m a coarsening of material may relate to relocation of the active river closer to the site. Large floods are recorded ($Z > 4$), but events near the bottom of the core may have been amplified by the open channel connection conveying coarser material. No clear trends in contaminant metal concentration were observed, but a slight increase in Zn levels occurred in the upper 2 m. Although 1953 should have been the last flood to occupy the site, the first coarse flood unit is only found at c. 1 m depth. Above this level, the infilling might relate to more recent local runoff. The two events around 1 m depth are therefore probably the 1956 (2513 m^3s^{-1}) and 1953 (3176 m^3s^{-1}) floods. A flood-rich episode between 1898 and 1907 can be related to an interval with frequent coarse flood units between 2 and 2.5 m. Other smaller peaks between 1953 and 1907 relate to floods of lesser magnitude (2000-2500 m^3s^{-1}), such as 1949, 1947, 1941, 1936, 1926, 1924, 1917, and 1913. The peak at 3.5 m has a relative magnitude appropriate for the 1880 event, while one of the coarsest flood units near the base of the channel fill is likely to be related to the 1857 flood. This matches the inferred age of abandonment before 1859.

4.4.3 Opiki

Opiki (Figs. 7, A8) was abandoned before 1859 (inferred from river position in 1859; Manawatu Catchment Board, 1982) and records floods up to 1953 when it was disconnected from the active floodplain by stopbank construction. The pollen biomarker at ca. 2.25 m recording exotic species (post-European settlement) appears to conflict with the radiocarbon age of 1745-1585 cal. BP at a depth of c. 2.5 m in this core. European indicators (*Rumex*, *Taraxacum*) first appear between 225 and 218 cm in the Opiki core, with pine pollen appearing at 180 cm. No sedimentary or pedogenic evidence for a hiatus has been observed, suggesting incorporation of aged carbon in the radiocarbon date. This is the only site positioned downstream of the Oroua confluence. The channel fill shows a typical abandonment sequence, with initially coarse deposits that grade into fine overbanks. Some variability in general overbank coarseness could be attributed to changes in the position of the active river, although given the low energy fluvial environment in this part of the system changes could also reflect discrete inputs from the nearby Oroua tributary. A number of large events are visible in the upper metre, with a flood unit very near to the surface. Because the stopbanks were constructed in the 1960s, this is very likely to be the 1953 event. Apart from the 1953 flood, a cluster of events between 70 and 90 cm are probably the 1897, 1902, and 1907 floods. The older part of the record is difficult to

resolve; nonetheless, such information is useful in demonstrating that very large floods also occurred in the period before large-scale deforestation.

4.3.4 Rocket

Rocket (Figs. 7, A9) is the most distal palaeochannel in the low-gradient reach of the river and records floods up to 1953. It was abandoned before 1859 (inferred from river position in 1859; Manawatu Catchment Board, 1982). The radiocarbon age of 2850-2792 cal. BP suggests a likely ~3 ka record of floods from this location. No European pollen indicators were observed in the samples from the Rocket site, suggesting that this site was mostly infilled prior to ca. A.D. 1840. However, notably the upper 50 cm of the record was not sampled as a consequence of oxidation. Two bulk radiocarbon dates yielded ages of 2831-2775 cal BP at 3.85-3.90 m depth and 2850-2792 cal BP at 2.99-3.04 m depth. Deposits are all finely laminated overbank sediments, with gravel occurring below 5 m (not scanned). The upper 3.5 m is more fine-grained with a gradual coarsening upward, possibly related to the river migrating toward the site. Larger floods are evenly distributed throughout the core. High Zn concentrations linked to contamination were recorded at c. 50 cm. If the coarse flood unit around 1.5 m is the 1857 event, this sedimentary sequence provides evidence of several other large floods in the realm of 3500-4000 m^3s^{-1} in the earlier part of the nineteenth century and potentially also in the eighteenth century.

4.4 Comparison between major documented floods (1800-2015) and palaeoflood record

Z-scores are site dependent, even for sites in the same reach of a river system, because they represent an offset compared with an average value, which differs given proximity effects and specific dynamics of channel infilling. Therefore, to compare flood *Z*-scores between locations, a statistical recurrence time is more useful. Additionally, a recurrence time can be compared with statistics of the gauged series, and allows us to test the relationship between major documented floods (ca. 1850-2015) in the Manawatu with the palaeoflood series. In the overbank palaeoflood sequence for the local records, where we have best time control and event dating, we regressed the *Z*-scores versus their statistical occurrence-time period of overbank section divided by the number of events exceeding a certain *Z*-score (Eq. 1):

$$RI = \frac{y}{n} \quad (1)$$

501 where RI is Recurrence interval (years), *y* is time span in overbank section, *n* is number of events
502 exceeding a given *Z*-score.

503

504 To avoid jumps in the data (if for example a gap exists in *Z*-scores series, leading to unequally spaced
505 data) and to get a realistic estimate on the RI of the largest *Z*-score measured, we fitted a regression
506 function through the estimated RIs vs. *Z*-scores. From these curves (Table 4) we recalculated the RI of
507 all measured *Z*-scores. This procedure worked for all sites with the exception of Palmy Park, where a
508 strong fining-upward trend complicates the by-proxy relative magnitude identification of discrete
509 large flood events on the basis of grain size. The results of this analysis demonstrate a good
510 relationship between recurrence estimates based on the discharge series and the recurrence
511 estimates based on the Manawatu palaeoflood record (Fig. 9). This confirms the robustness of using
512 grain size as a proxy for estimating the relative magnitudes of palaeofloods in the Manawatu.

513 **Table 4**

514 *Z*-score versus recurrence time regression analysis for overbank deposits ca. 1800-2015 for the
515 Manawatu palaeoflood sites.

Site	***Regression function***	***R^2***	***Registration period A.D. (used for correlation)***	***Avg SAR (mm/y)***	***Core section (cm)***
Alpaca	$0.1040e^{(2.1811x)}$	*0.99*	*c. 1800-1900 (100 years)*	*17*	*35-200*
Hamilton 1	$0.0163e^{(1.9793x)}$	*0.90*	*1942-1991 (49 yearrs)*	*54*	*120-385*
Hamilton 2	$0.0864e^{(1.2764x)}$	*0.97*	*c. 1870-1970 (100 years)*	*45*	*0-450*
Karere 2	$0.1392e^{(1.2642x)}$	*0.97*	*1897-2000 (103 years)*	*26*	*0-265*
Napier Road	$1.9411e^{(0.5766x)}$	*0.97*	*c. 1800-2015 (215 years)*	*8*	*30-200*
Opiki	$0.7596e^{(0.6035x)}$	*0.79*	*c. 1855-1955 (100 years)*	*15*	*0-150*
Palmy Park	$0.0161e^{(3.1969x)}$	*0.94*	*c. 1890-1970 (80 years)*	*9*	*65-130*
Riverside Drive	$0.2272e^{(1.908x)}$	*0.98*	*1860-2005 (145 years)*	*10*	*0-150*
Rocket	$0.1156e^{(1.4627x)}$	*0.99*	*1960-1850 (110 years)*	*12*	*30-160*

516

517 **Figure 9**

5. Discussion and Conclusions

The sedimentary archive provided by palaeochannels in the lower Manawatu floodplain provides a high resolution and a long-term record of historic and prehistoric floods in the Manawatu catchment. This record is the first to provide an indicator of timing and of magnitude of discrete, storm-generated flood events in New Zealand in the late Holocene. The records from the distal palaeochannel at Napier Road (Figs. 6, 8), which has secure age control back as far as 2000 cal. YBP, suggests that historical floods are among the largest to have occurred in the Manawatu in the past 2000 years. Furthermore, of these floods, the largest estimated in excess of 4000 m^3s^{-1} in 1857 has not yet been surpassed and may well represent the largest in ~3000 years. The timing of such large flood events in the mid- and late-1800s is consistent with observations elsewhere in New Zealand where for example widespread deforestation in the Motueka catchment in the 1870s was followed by severe flooding and substantial erosion (Beatson and Whelan 1993). A link between land cover change and changing flood magnitude and frequency is likely, since clearance of trees from a catchment increases the catchment runoff coefficient. Furthermore the end of the nineteenth century has been classified as a period of enhanced river activity in New Zealand (Fuller et al.,, 2015), associated not only with human disturbance of catchments but also enhanced storminess (Norton et al., 1989) and neoglacial activity (Schaefer et al., 2009); and an enhanced southwesterly flow across New Zealand has been reconstructed during the Little Ice Age in New Zealand (Lorrey et al., 2014). Land cover changes and climate regime would appear to be favourable in generating large floods in the Manawatu catchment at this time.

Nonetheless, what the record presented here does imply is the absence of any particularly large or catastrophic flood event in the Manawatu during the past ~3000 years based on the nine sites in the ~20-km-long study reach. Several '200-year' floods (~4500 m^3s^{-1}) are likely, but nothing larger. The implication of this is that the extended Manawatu flood series indicates a relatively stable flood regime in this catchment or an upper physical boundary to meteorological events. This limit may be imposed by the Manawatu Gorge, which acts as a 'throttle' on floods generated from the eastern subcatchments (Manawatu Catchment Board, 1983), with the result that floodwaters pond to the east of the Gorge. The Manawatu flood series presented here does not appear to have been marked by notable variability in flood magnitude and frequency during the last two millennia. This may reflect the nature of the catchment, straddling as it does the coherent precipitation regions of the southwestern North Island and eastern North Island (Mullan 1998) whose boundary is the axial ranges, which may insulate the lower reaches of the catchment from extreme floods. However, comparison

with the CPF curve for the North Island does indicate that a number of flood-rich periods occurred in the past 2000 years (Fig. 6), at ca. 2300, 2100, 1700-1600, 750, 450-350, 150, and 80 cal. YBP.

The floodplain sedimentary archive presented here shows an acceleration in floodplain sedimentation following European forest clearance in the catchment. At the Rocket site, a sedimentation rate between ca. 870 B.C. and AD 1857 of 0.57 mm y^{-1} compares with a rate of 9.49 mm yr^{-1} after 1857 (cf. Fig. 8). Extremely high rates of sedimentation were observed in the stopbanked floodplain at Hamilton 1 (58 mm y^{-1}), where stopbanks constrain floodplain sedimentation resulting in aggradation and the development of a perched floodplain. This greatly exceeds more modest rates of 9.5 mm y^{-1} recorded since 1857 at Riverside Drive, where the floodplain is not stopbanked and flood deposits are more widely dispersed. This relatively modest sedimentation rate (9.5 mm y^{-1}) corresponds with floodplain sedimentation rates elsewhere in New Zealand following post-settlement catchment disturbance (Richardson et al., 2014). The implications for palaeoflood reconstruction are that a very high resolution of floods is preserved since the 1800s, but probably only the largest floods register a clear sedimentary signature in the record prior to this, particularly in distal cores. This weaker sedimentary signature, together with limited means of constraining ages in these cores, presents challenges for palaeoflood reconstruction in the Manawatu record.

As a proof of concept, the results presented in this paper demonstrate that high resolution flood records can be reconstructed from XRF core scanning. This also provides a useful insight into understanding magnitude and frequency of very large floods, which is essential for flood risk assessment in a changing climate.

Acknowledgements

Funding for this research was provided by the 2015 Massey University Research Fund to ICF, MGM and KAH. WHJT was supported by a NWO Rubicon grant (825.14.005). We thank David Feek (Physical Geography Technician, SAE) for assistance with fieldwork. Ian Saunders (Aberystwyth University) is acknowledged for supporting the grain-size analyses. Horizons Regional Council are thanked for providing the LiDAR data set (Andrew Steffert), flood modelling data (Jon Bell), and additional archive information (Jeff Watson). We thank the reviewers tasked with reviewing this manuscript, and the especially helpful comments of an anonymous referee and the Editor, Richard Marston.

References

Beatson, K.E. & Whelan, H. (1993). *The River Flows on: Ngatimoti Through Flood and Fortune*. K. Beatson & H. Whelan.

583 Clement, A.J., Sloss, C.R. & Fuller, I.C. (2010). Late quaternary geomorphology of the Manawatu
584 coastal plain, North Island, New Zealand. *Quaternary International*, 221, 36-45.
585 Clement, A.J.H., Fuller, I.C. & Sloss, C. (2017). Facies architecture, morphostratigraphy, and
586 sedimentary evolution of a rapidly-infilled Holocene incised-valley estuary: the lower
587 Manawatu valley, North Island New Zealand. Marine Geology, in press.
588 Cowie CA (1957). Floods in New Zealand 1920-1953. The Soil Conservation and Rivers Control Council,
589 Wellington.
590 Ely, L.L. (1997). Response of extreme floods in the southwestern United States to climatic variations
591 in the late Holocene. *Geomorphology*, 19, 175-201.
592 Foulds, S.A. & Macklin, M.G. (2016). A hydrogeomorphic assessment of twenty-first century floods in
593 the UK. *Earth Surface Processes and Landforms*, 41, 256-270.
594 Fuller, I.C., Macklin, M.G. & Richardson, J.M. (2015). The geography of the Anthropocene in New
595 Zealand: Differential river catchment response to human impact. *Geographical Research*, 53,
596 255-269.
597 Fuller, I.C., Basher, L. & Macklin, M.G. (2016). Natural Hazards, in: Jellyman P, Davie TJA, Pearson CP,
598 Harding JS (Eds) Advances in New Zealand Freshwater Science, 415-443.
599 Graettinger, A.H., Manville, V. & Briggs, R.M. (2010). Depositional record of historic lahars in the upper
600 Whangaehu Valley, Mt. Ruapehu, New Zealand: implications for trigger mechanisms, flow
601 dynamics and lahar hazards. *Bulletin of volcanology*, 72, 279-296.
602 Henderson, R. & Diettrich, J. (2007). Statistical analysis of river flow data in the Horizons Region. NIWA
603 Christchurch, New Zealand.
604 Hicks, D.M., Shankar, U., McKerchar, A.I., Basher, L., Lynn, I., Page, M. *et al.* (2011). Suspended
605 sediment yields from New Zealand rivers. *Journal of Hydrology (New Zealand)*, 81-142.
606 Hogg, A.G., Hua, Q., Blackwell, P.G., Niu, M., Buck, C.E., Guilderson, T.P. *et al.* (2013). SHCal13 Southern
607 Hemisphere calibration, 0–50,000 years cal BP. *Radiocarbon*, 55, 1889-1903.
608 Jones, A.F., Macklin, M.G. & Brewer, P.A. (2012). A geochemical record of flooding on the upper River
609 Severn, UK, during the last 3750years. *Geomorphology*, 179, 89-105.
610 Kiem, A.S., Franks, S.W. & Kuczera, G. (2003). Multi-decadal variability of flood risk. *Geophysical*
611 *Research Letters*, 30.
612 Leigh, D.S., 2017. Vertical accretion sand proxies of gaged floods along the upper Little Tennessee
613 River, Blue Ridge Mountains, USA. Sedimentary Geology,
614 https://doi.org/10.1016/j.sedgeo.2017.09.007
615 LoRe, G., Fuller, I.C., Tarolli, P. & Sofia, G. High-resolution mapping of Manawatu palaeochannels. New
616 Zealand Geographer, in review.
617 Lorrey, A., Fauchereau, N., Stanton, C., Chappell, P., Phipps, S., Mackintosh, A. *et al.* (2014). The Little
618 Ice Age climate of New Zealand reconstructed from Southern Alps cirque glaciers: a synoptic
619 type approach. *Climate Dynamics*, 42, 3039.
620 Macklin, M. G., Rumsby, B. T., & Newson, M. D. (1992). Historical floods and vertical accretion of fine-
621 grained alluvium in the Lower Tyne Valley, northeast England. Dynamics of gravel-bed rivers,
622 573-589.
623 Macklin, M.G., Fuller, I.C., Jones, A.F. & Bebbington, M. (2012). New Zealand and UK Holocene flooding
624 demonstrates interhemispheric climate asynchrony. *Geology*, 40, 775-778.
625 MANAWATU CATCHMENT BOARD, 1982: 'History of the Manawatu River and the Manawatu
626 Catchment Board'. Manawatu Catchment Board Report No. 42.
627 MANAWATU CATCHMENT BOARD, 1983: 'Lower Manawatu scheme review, 1950- 1982 and proposed
628 works, 1983-1988'. Manawatu Catchment Board Report No. 50.
629 Manville, V. (2004). Palaeohydraulic analysis of the 1953 Tangiwai lahar; New Zealand's worst volcanic
630 disaster. *Acta Vulcanologica*, 16, 1000-1015.
631 Manville, V. & Hodgson, K. (2011). Paleohydrology of volcanogenic lake break-out floods in the taupo
632 volcanic zone, new zealand. *Natural and Artificial Rockslide Dams*, 519-541.

633 Manville, V. & Wilson, C.J.N. (2004). The 26.5 ka Oruanui eruption, New Zealand: A review of the roles
634 of volcanism and climate in the post-eruptive sedimentary response. *New Zealand Journal of*
635 *Geology and Geophysics*, 47, 525-547.
636 Manville, V., White, J., Houghton, B. & Wilson, C. (1999). Paleohydrology and sedimentology of a post–
637 1.8 ka breakout flood from intracaldera Lake Taupo, North Island, New Zealand. *Geological*
638 *Society of America Bulletin*, 111, 1435-1447.
639 Manville, V., Newton, E.H. & White, J.D. (2005). Fluvial responses to volcanism: resedimentation of
640 the 1800a Taupo ignimbrite eruption in the Rangitaiki River catchment, North Island, New
641 Zealand. *Geomorphology*, 65, 49-70.
642 McGlone, M. and Wilmshurst, J. (1999) Dating initial Maori environmental impact in New Zealand.
643 Quaternary International 59: 5-16.
644 Moore PD, Webb JA, Collinson ME (1991) Pollen Analysis. 2nd ed. Blackwell Scientific Publications,
645 London.
646 Mullan, A. (1998). Southern Hemisphere sea-surface-temperatures and their contemporary and lag
647 association with New Zealand temperature and precipitation. *International Journal of*
648 *Climatology*, 18, 817-840.
649 Munoz, S.E., Gruley, K.E., Massie, A., Fike, D.A., Schroeder, S. & Williams, J.W. (2015). Cahokia's
650 emergence and decline coincided with shifts of flood frequency on the Mississippi River.
651 *Proceedings of the National Academy of Sciences*, 112, 6319-6324.
652 NIWA (2017) National and Regional Climate maps, available at:
653 https://www.niwa.co.nz/climate/national-and-regional-climate-maps/manawatu. Accessed
654 19 July 2017.
655 Norton, D., Briffa, K. & Salinger, M. (1989). Reconstruction of New Zealand summer temperatures to
656 1730 AD using dendroclimatic techniques. *International Journal of Climatology*, 9, 633-644.
657 Page, C.F., 1994. Manawatu River at Fitzherbert. Manawatu Wanganui Regional Council Report
658 94/EXT/160.
659 Page, K. & Heerdegen, F.G. (1985). Channel change on the lower Manawatu River. *New Zealand*
660 *Geographer*, 41, 35-38.
661 Pillans, B., 1986. A late Quaternary uplift map for the North Island, New Zealand. Royal Society of New
662 Zealand Bulletin 24, 409-417.
663 Richardson, J., Fuller, I., Macklin, M., Jones, A., Holt, K., Litchfield, N. *et al.* (2013). Holocene river
664 behaviour in New Zealand: response to regional centennial-scale climate forcing. *Quaternary*
665 *Science Reviews*, 69, 8-27.
666 Richardson, J., Fuller, I.C., Holt, K.A., Litchfield, N.J & Macklin, M.G. (2014). Rapid post-settlement
667 floodplain accumulation in Northland, New Zealand. *Catena*, 113, 292-305.
668 Schaefer, J.M., Denton, G.H., Kaplan, M., Putnam, A., Finkel, R.C., Barrell, D.J. *et al.* (2009). High-
669 frequency Holocene glacier fluctuations in New Zealand differ from the northern signature.
670 *science*, 324, 622-625.
671 Toonen, W., Winkels, T., Cohen, K., Prins, M. & Middelkoop, H. (2015). Lower Rhine historical flood
672 magnitudes of the last 450years reproduced from grain-size measurements of flood deposits
673 using End Member Modelling. *Catena*, 130, 69-81.
674 Toonen, W.H.J., Middelkoop, H., Konijnendijk, T.Y.M., Macklin, M.G. & Cohen, K.M. (2016). The
675 influence of hydroclimatic variability on flood frequency in the Lower Rhine. *Earth Surface*
676 *Processes and Landforms*, 41, 1266-1275.
677 Toonen, W.H.J., Foulds, S.A., Macklin, M.G. & Lewin, J. (2017). Events, episodes, and phases: Signal
678 from noise in flood-sediment archives. *Geology*, 45, 331-334.
679 Turner, J.N., Jones, A.F., Brewer, P.A., Macklin, M.G. & Rassner, S.M. (2015). Micro-XRF Applications
680 in Fluvial Sedimentary Environments of Britain and Ireland: Progress and Prospects. In: *Micro-*
681 *XRF Studies of Sediment Cores*. Springer, pp. 227-265.

Vale, S., Fuller, I., Procter, J., Basher, L. & Smith, I. (2016). Characterization and quantification of suspended sediment sources to the Manawatu River, New Zealand. *Science of the Total Environment*, 543, 171-186.
Wellman, H.W., 1972. Rate of horizontal fault displacement in New Zealand. Nature 237, 275-277.
Whitehouse, I.E., Pearce, A.J., 1992. Shaping the mountains of New Zealand, in: Soons, J.M., Selby, M.J. (Eds.), Landforms of New Zealand. Longman Paul, Auckland, pp. 144-160.
Willis G 2014. Managing natural hazards in New Zealand: towards more resilient communities: a thinkpiece. October 2014. Available at: http://www.lgnz.co.nz/assets/Publications/Managing-natural-hazards-LGNZ-think-piece.pdf (accessed 5 July 2017).
Wilmshurst, J. (1997). The impact of human settlement on vegetation and soil stability in Hawke's Bay, New Zealand. New Zealand Journal of Botany 35: 97 – 111.

List of Figures

Fig. 1. Manawatu catchment: (A) North Island location, (B) primary sub-catchments and location of Palmerston North (the focus of this study), (C) catchment land use, (D) catchment geology (after Vale et al., 2016). Rectangle shows extent of study area (cf. Fig. 2).

Fig. 2. I. Airborne laser scanning (LiDAR) derived terrain surface of the lower Manawatu valley in the vicinity of Palmerston North (data supplied courtesy of Horizons Regional Council). The urban area of Palmerston North is outlined. Photos (A-C) give examples of palaeochannels: (A) is located at the northern margin of the floodplain adjacent to a late Pleistocene river terrace (Napier Road); (B) is the former McRaes Bend, which was artificially cut in the 1950s for city flood protection; (C) is Hamilton's lagoon in the naturally unconfined floodplain (Hamilton 2). II. Larger-scale image of the Manawatu floodplain showing location of core sites and cross sections of the floodplain, with cored palaeochannels labelled.

Fig. 3. Grain size comparisons. (A) D_{50}:D_{90} relationships for all sites; (B) comparison between normalised Zr/Rb ratio and D_{50}; (C) grain size data for an exemplar core (Hamilton 1, cf. Fig. 2), plotting D_{50} and D_{90} downcore and percentage clay, silt, and sand.

Fig. 4. Documented floods (largest annual daily maximum) in the Manawatu River at Palmerston North. Data supplied by Horizons Regional Council.

Fig. 5. Summary pollen diagrams for Hamilton 1, Napier Road, Palmy Park, and the Rocket and Opiki sites. Data are displayed as relative proportions calculated against the sum of all dryland pollen, which includes trees, shrubs, and herbs (natives and exotics) but excludes ferns.

Fig. 6. Active floodplain sites: *Z*-score results for Hamilton 1, Karere 2, Riverside Drive, and Napier Road compared with documented and gauged flood record for the Manawatu at Palmerston North,

attributed to the most likely flood event on the basis of radiometric age, pollen, contaminant metals, and cartographic sources. Example core photos are included. CPF curve (from Fuller et al., 2015) shown and linked to the Napier Road record using the ^{14}C age of 2050-1926 cal. YBP and the A.D. 1840 pollen age estimate. Flood-rich periods are identified as peaks exceeding 0.75.

Fig. 7. Inactive floodplain sites: Floods inferred using *Z*-scores for Palmy Park, Hamilton 2, Alpaca, Opiki, and Rocket compared with one another and the documented flood record, attributed to the most likely flood event on the basis of radiometric age, pollen, contaminant metals, and cartographic sources. The longer records from the upstream active floodplain sites (Riverside Drive and Napier Road) are also included for comparison. Example core photos are included.

Fig. 8. Schematic diagram showing the relative floodplain position and broad sedimentology of cores described in detail in the text. Dates of inferred floods are labelled.

Fig. 9. Recurrence time estimates of major floods based on observed discharge series (open circles) compared with reconstructed palaeofloods using *Z*-score regression as a proxy for grain size (diamonds). The *Z*-scores presented are an average derived from all sites in the Manawatu, excluding Palmy Park.

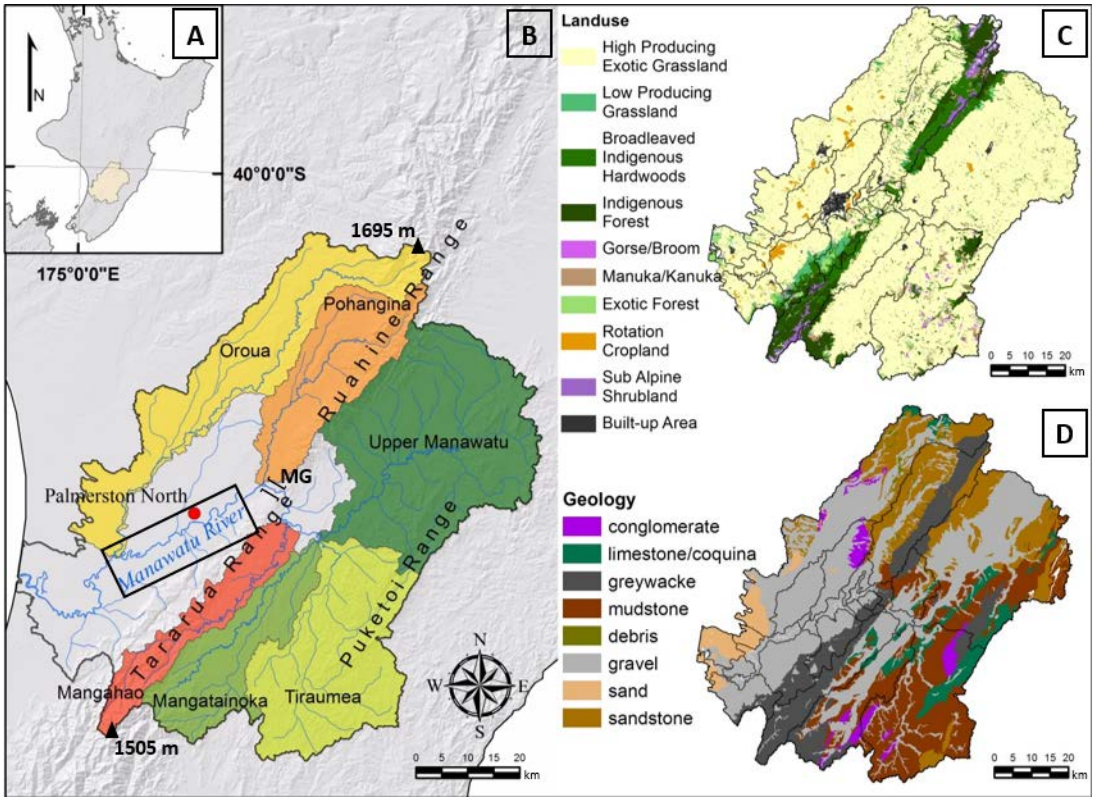
A
N
40°0'0"S
175°0'0"E
B
1695 m
Pohangina
Oroua
Ruahine Range
Upper Manawatu
MG
Palmerston North
Manawatu River
Tararua Range
Puketoi Range
Mangahao
Mangatainoka
Tiraumea
1505 m
N
W
E
S
0 5 10 15 20
km
Landuse
High Producing Exotic Grassland
Low Producing Grassland
Broadleaved Indigenous Hardwoods
Indigenous Forest
Gorse/Broom
Manuka/Kanuka
Exotic Forest
Rotation Cropland
Sub Alpine Shrubland
Built-up Area
C
0 5 10 15 20
km
D
Geology
conglomerate
limestone/coquina
greywacke
mudstone
debris
gravel
sand
sandstone
0 5 10 15 20
km

Figure 1.

I

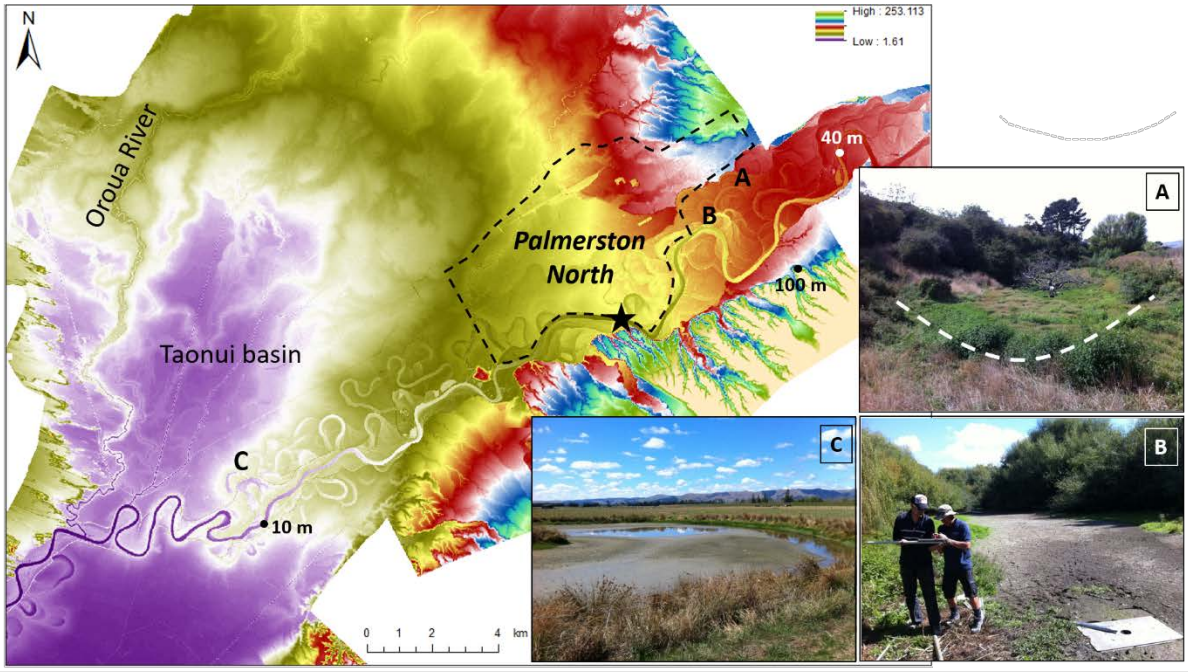

II

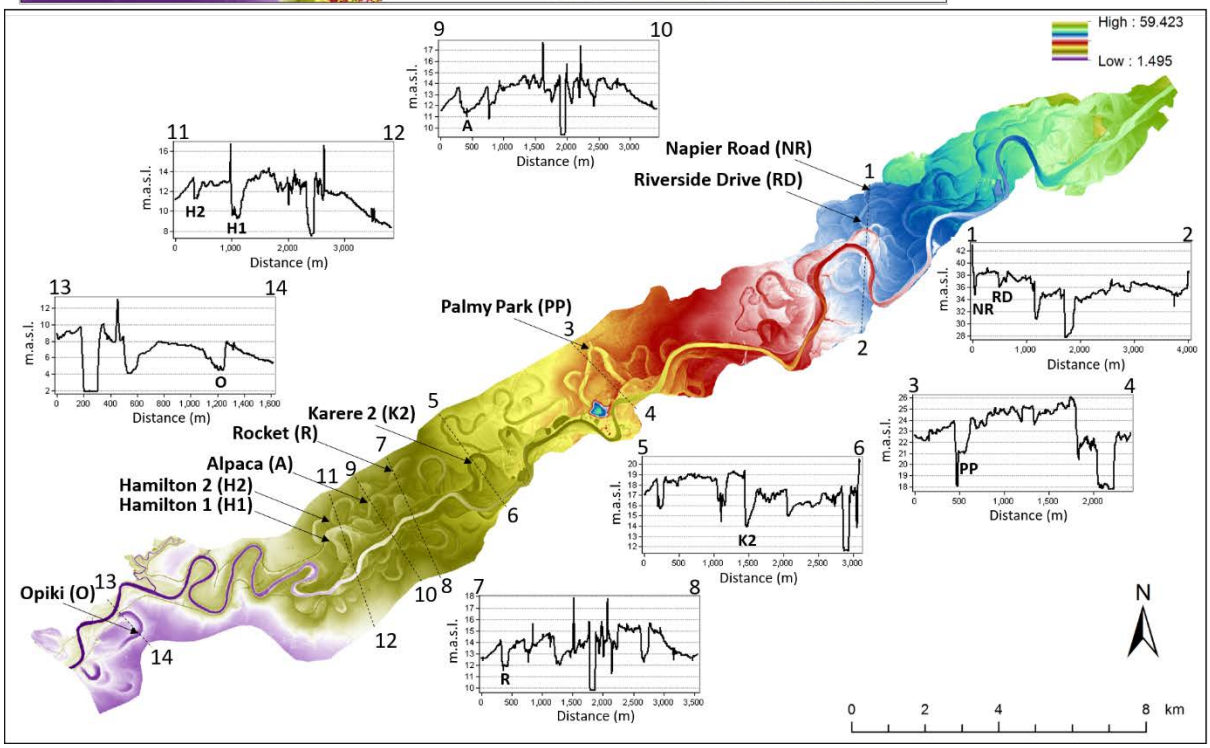

753

754 **Figure 2.**

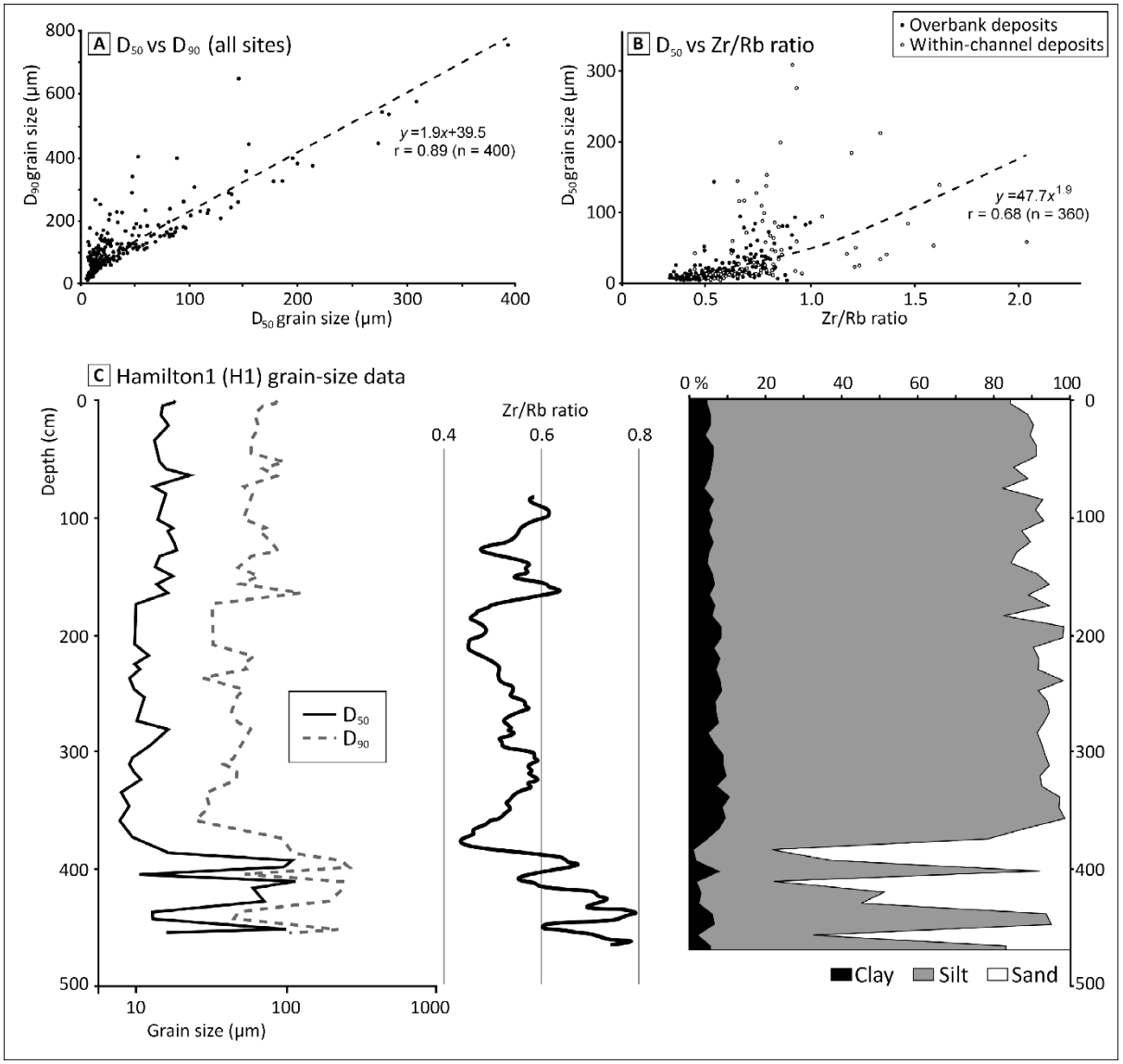
A D50 vs D90 (all sites)
D90 grain size (µm)
D50 grain size (µm)
y =1.9x+39.5
r = 0.89 (n = 400)
B D50 vs Zr/Rb ratio
• Overbank deposits
◦ Within-channel deposits
D50 grain size (µm)
Zr/Rb ratio
y =47.7x1.9
r = 0.68 (n = 360)
C Hamilton1 (H1) grain-size data
Depth (cm)
Zr/Rb ratio
D50
D90
Grain size (µm)
0 %
Clay
Silt
Sand

Figure 3.

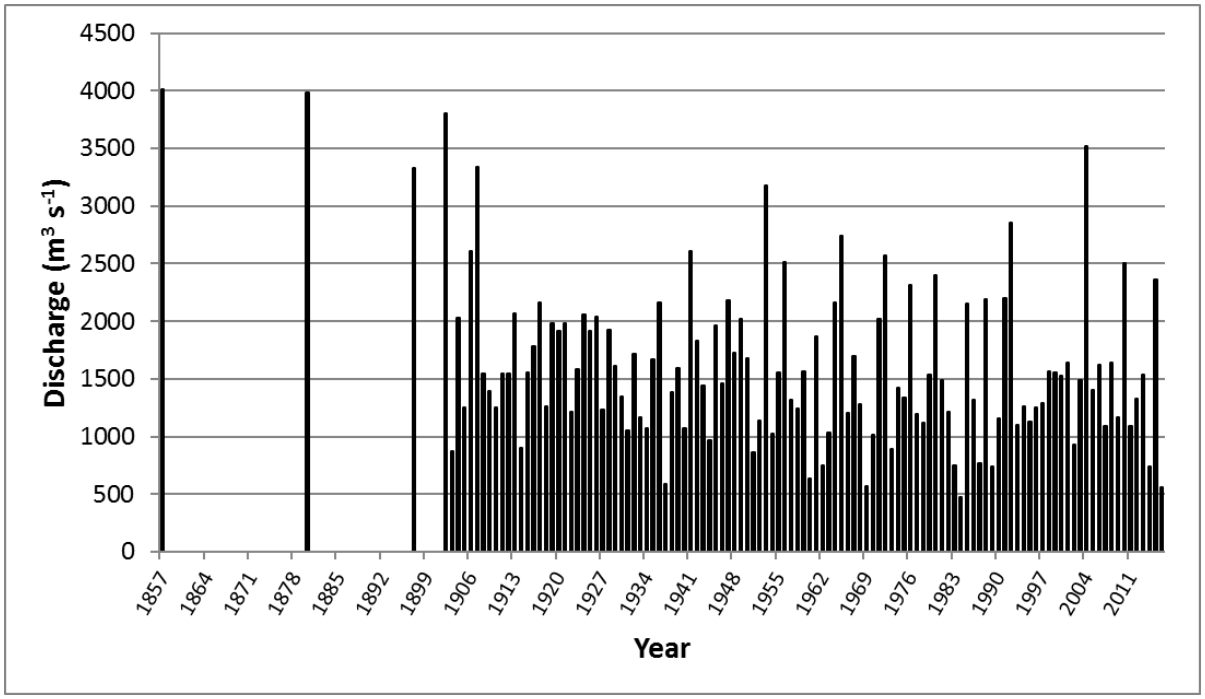
Discharge (m³ s⁻¹)
4500
4000
3500
3000
2500
2000
1500
1000
500
0
1857
1864
1871
1878
1885
1892
1899
1906
1913
1920
1927
1934
1941
1948
1955
1962
1969
1976
1983
1990
1997
2004
2011
Year

Figure 4.

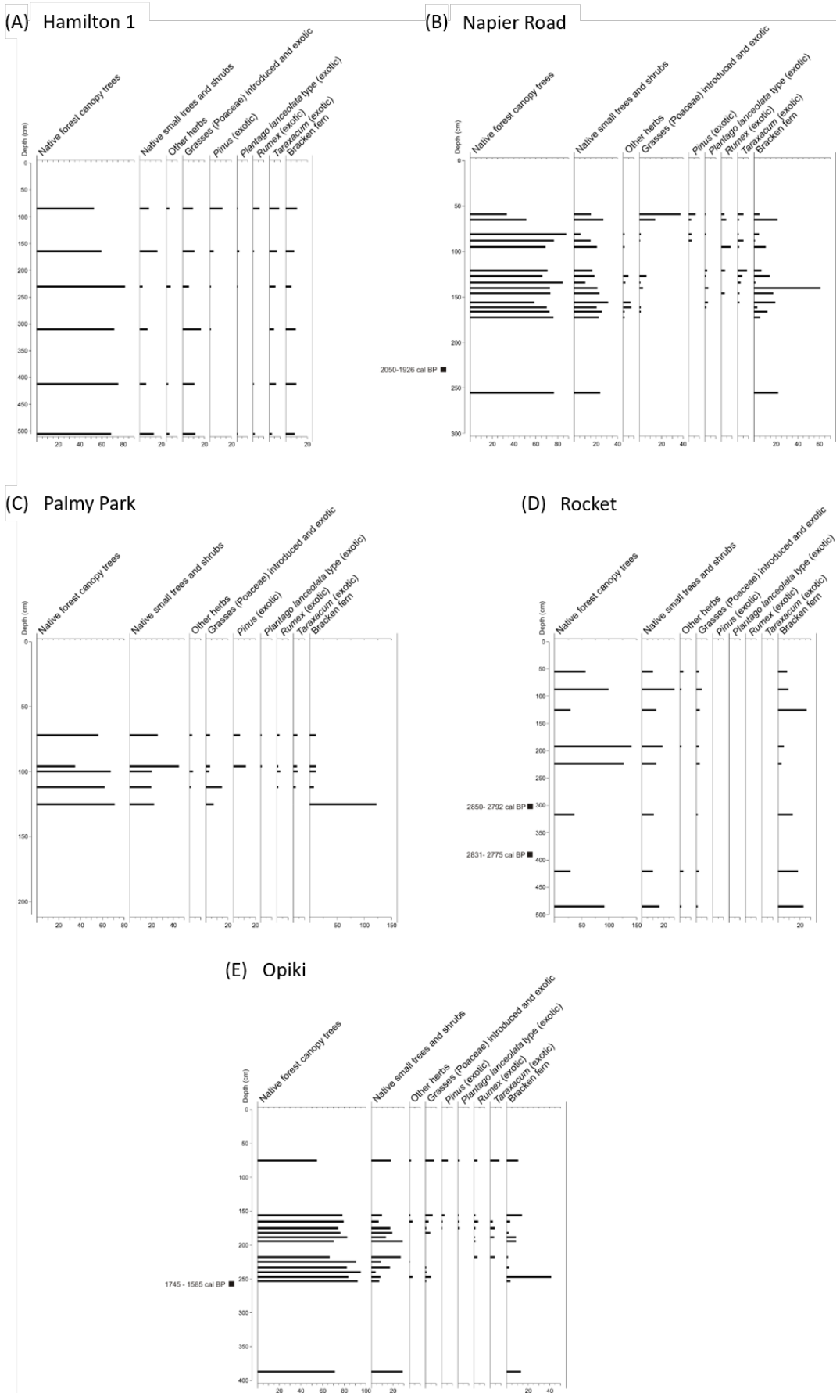

762

763 **Figure 5.**

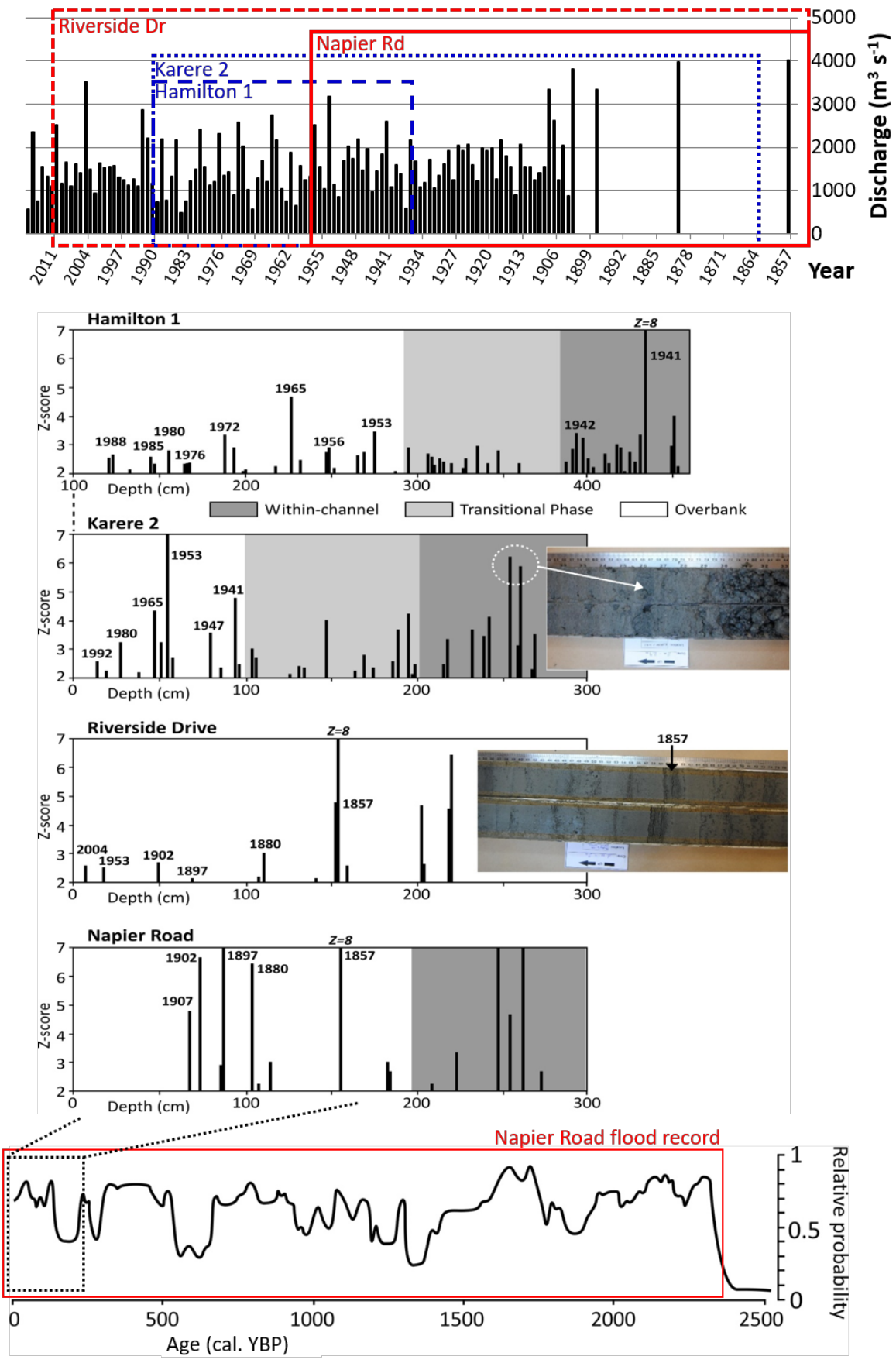

764

765 **Figure 6.**

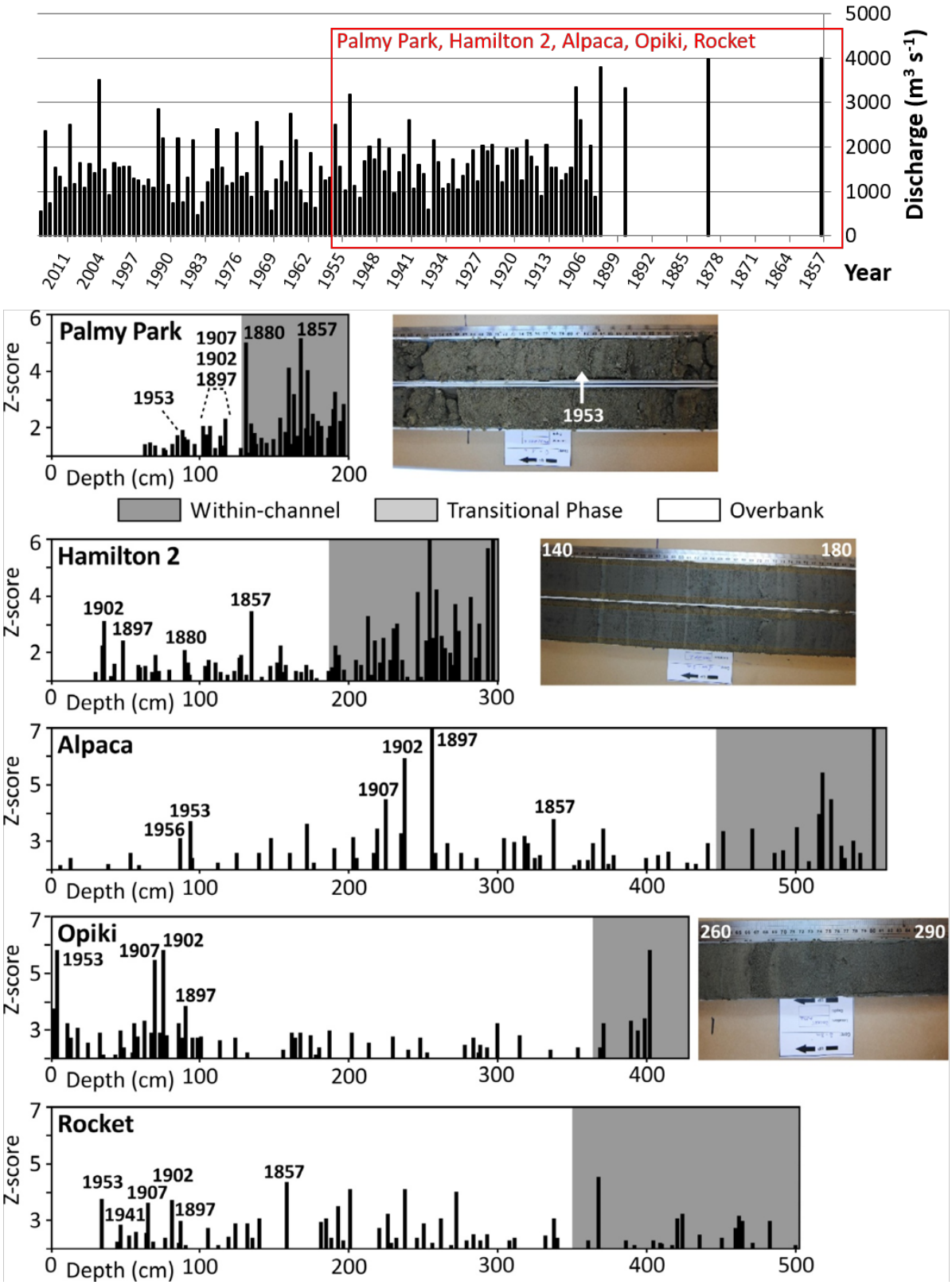

766

767 **Figure 7.**

768

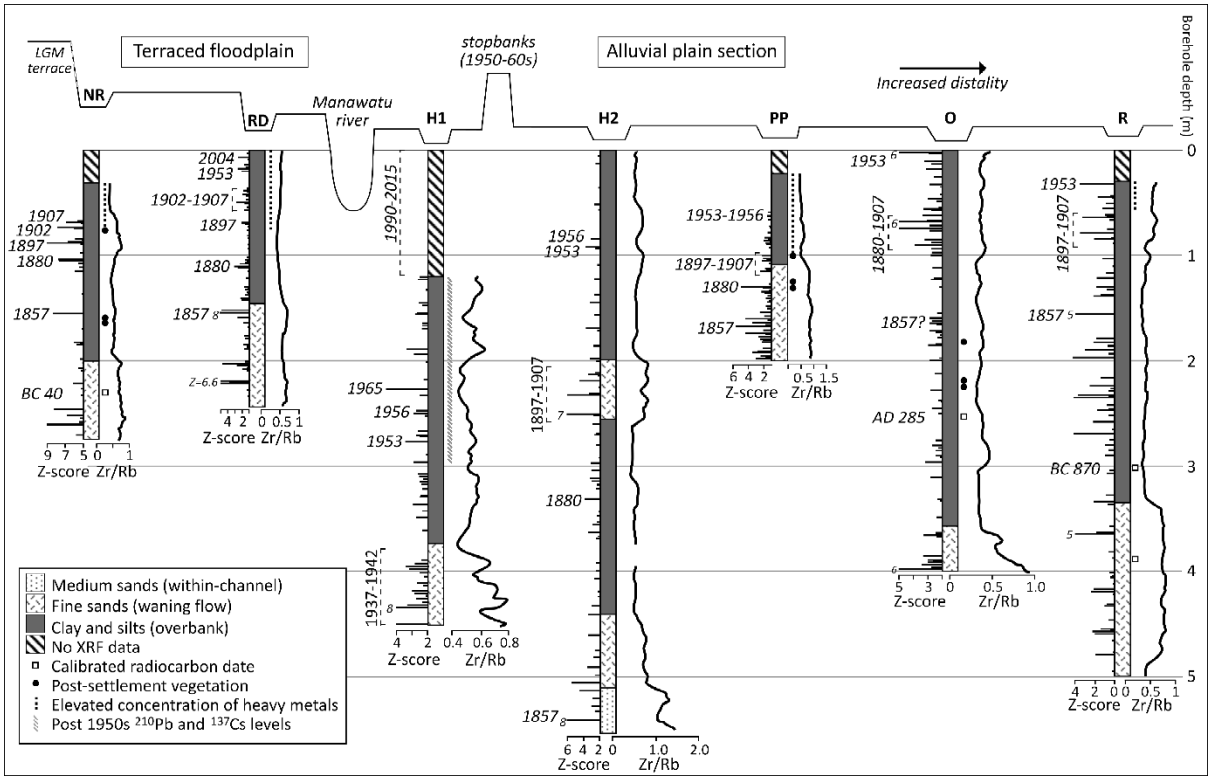

769

770 **Figure 8.**

771

772

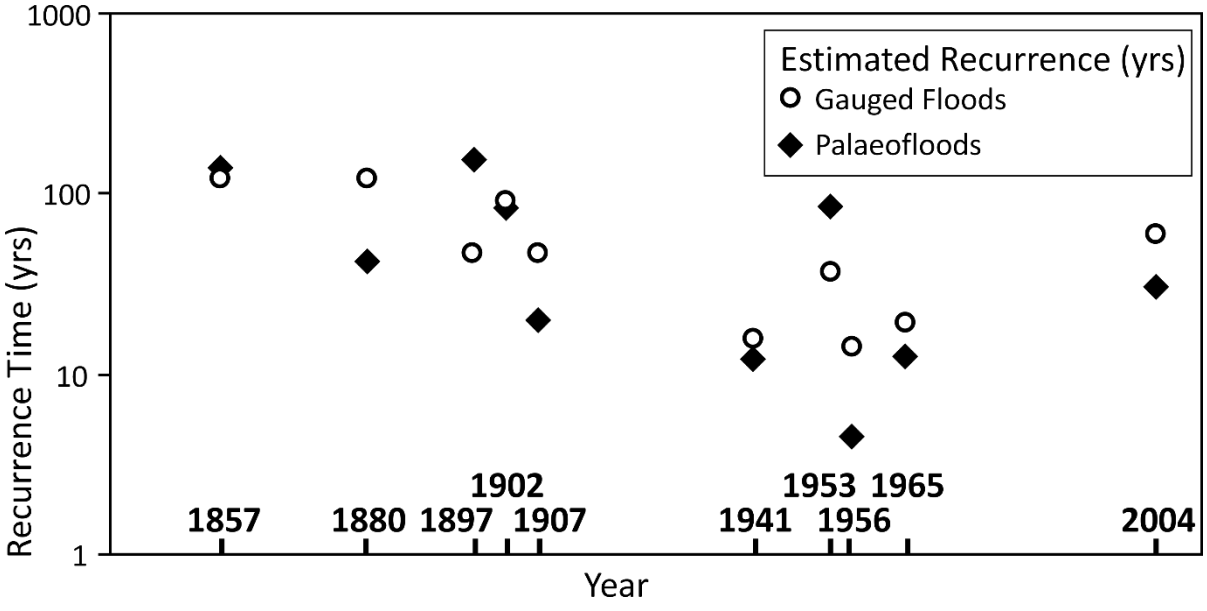

773

774 **Figure 9.**

775

776 **Appendix**

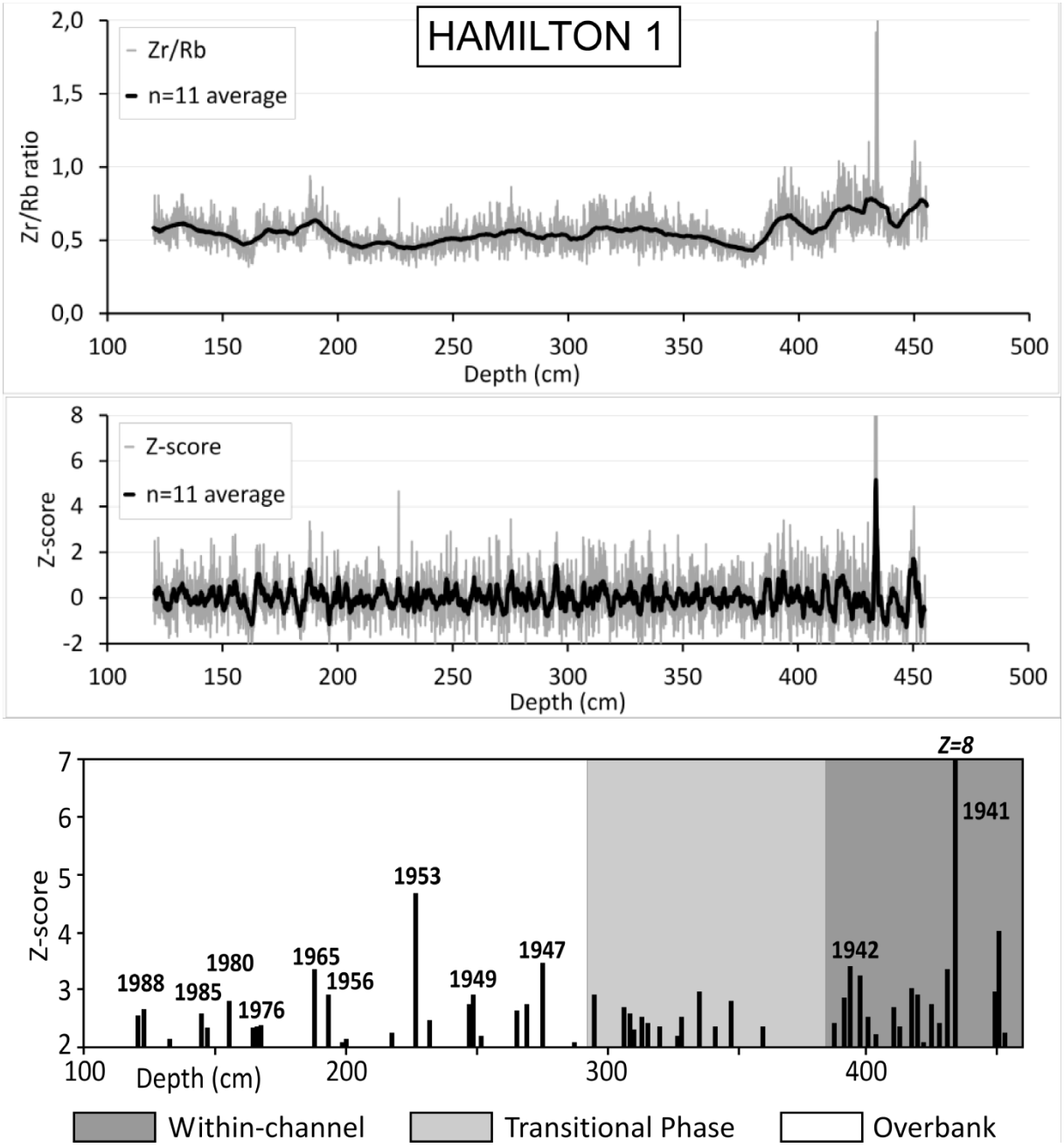

777

778

779

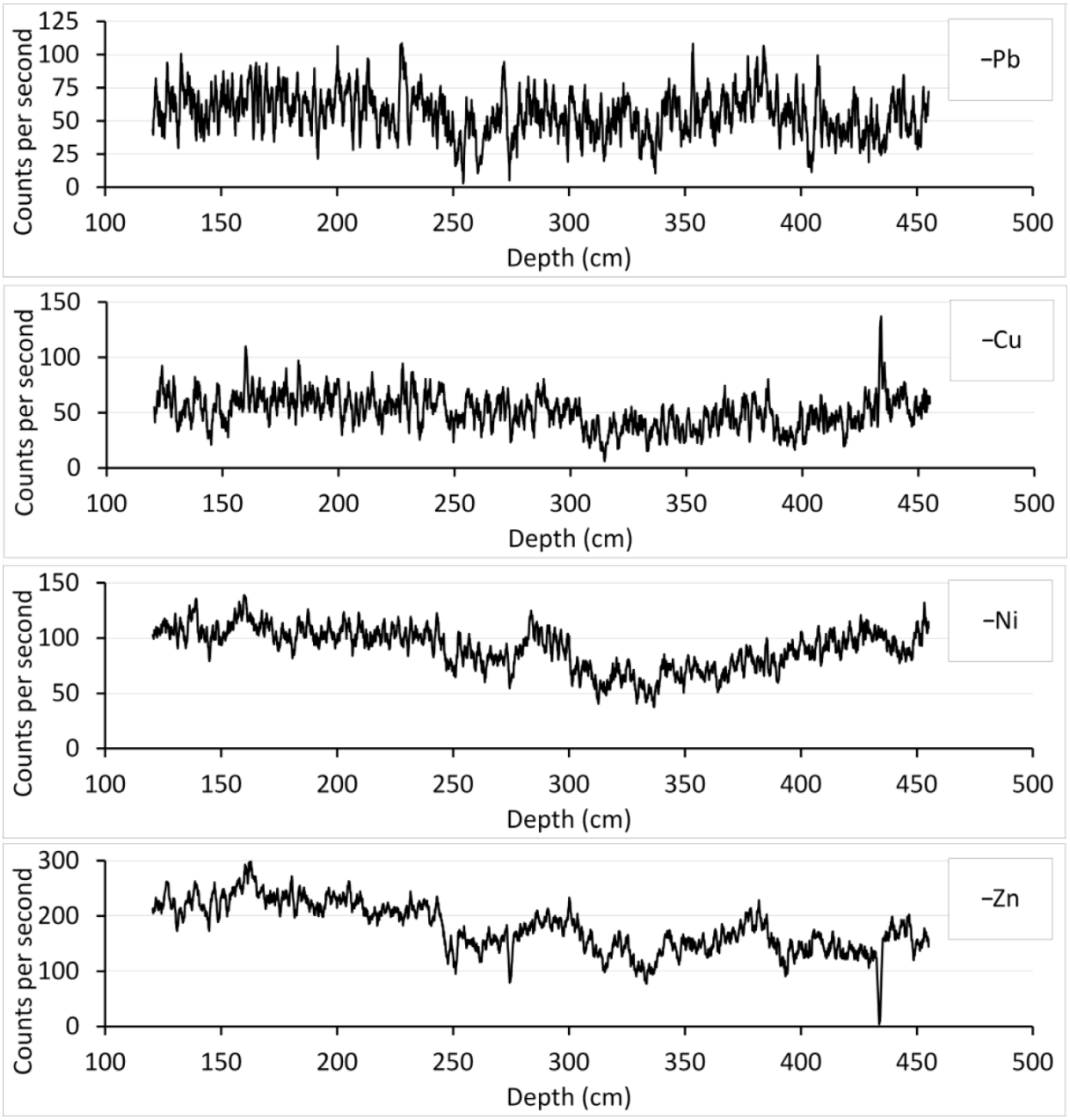

780

781 **Figure A1** Hamilton 1 core: Zr/Rb ratio, Z-score, inferred floods, heavy metal geochemistry (Pb, Cu,
782 Ni, Zn).

783

Karere 2

Karere 2 was abandoned shortly after 1860 (exact date not known, Manawatu Catchment Board, 1982) and can be flooded by small (2 yr ARI floods) (Table 1). Below 200 cm fairly coarse deposits gradually fine upward into overbank sediments in the upper 120 cm. Many smaller flood units were detected (Fig. 7). Gradually increasing Zn levels in the upper metre are partly related to an increase in fines, and cannot be considered as an indication for increasing pollution levels in the catchment. It is difficult to assign ages to flood deposits. The peak around 50 cm may well be the 1953 event. Peaks in the deeper part of the core might relate to the flood-rich episode between 1897-1907. Despite being actively flooded in recent decades because of the position of the palaeochannel inside the stopbanks, no flood unit could be related to the 2004 event as the recent units at this site are relatively fine-grained.

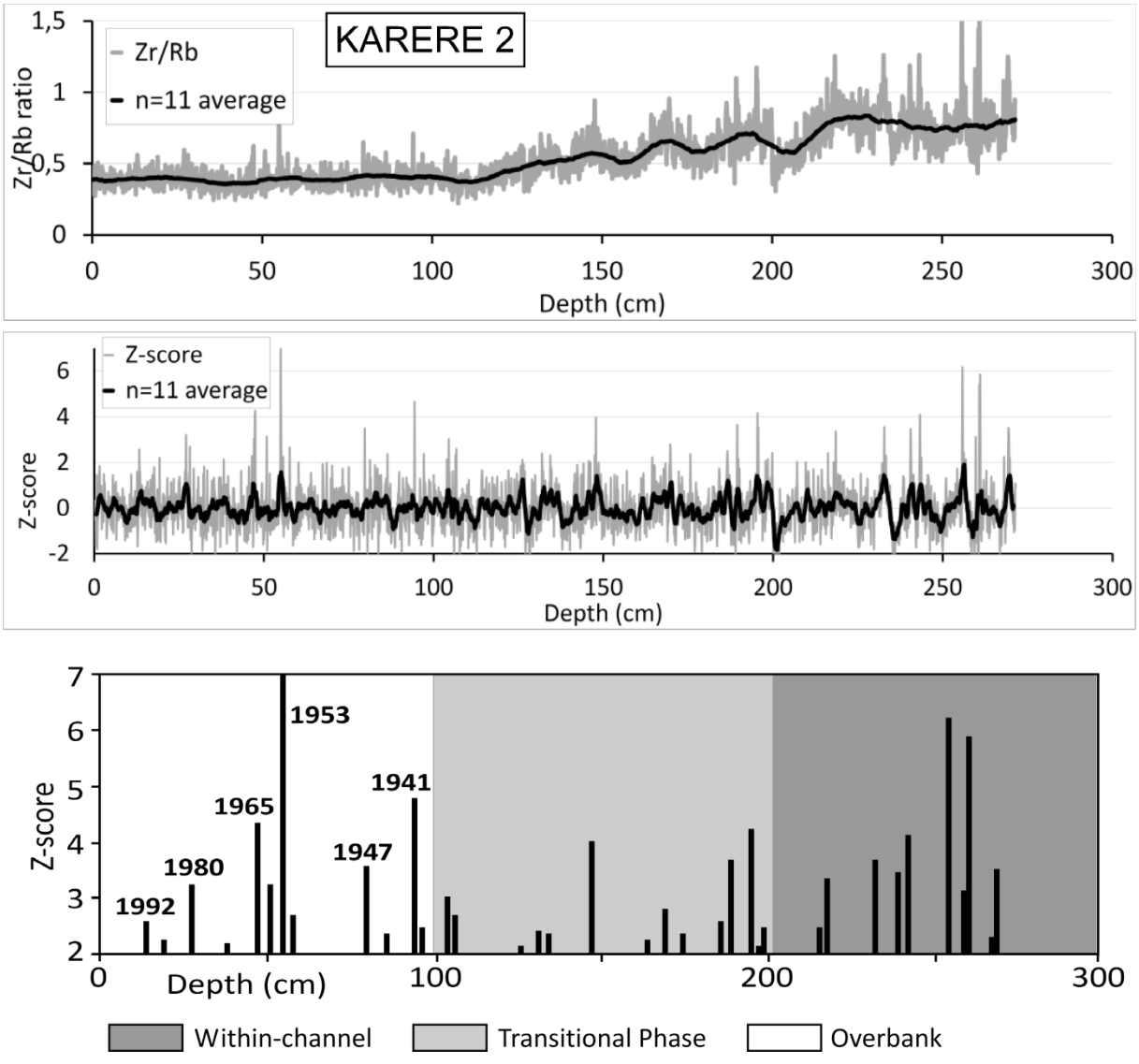

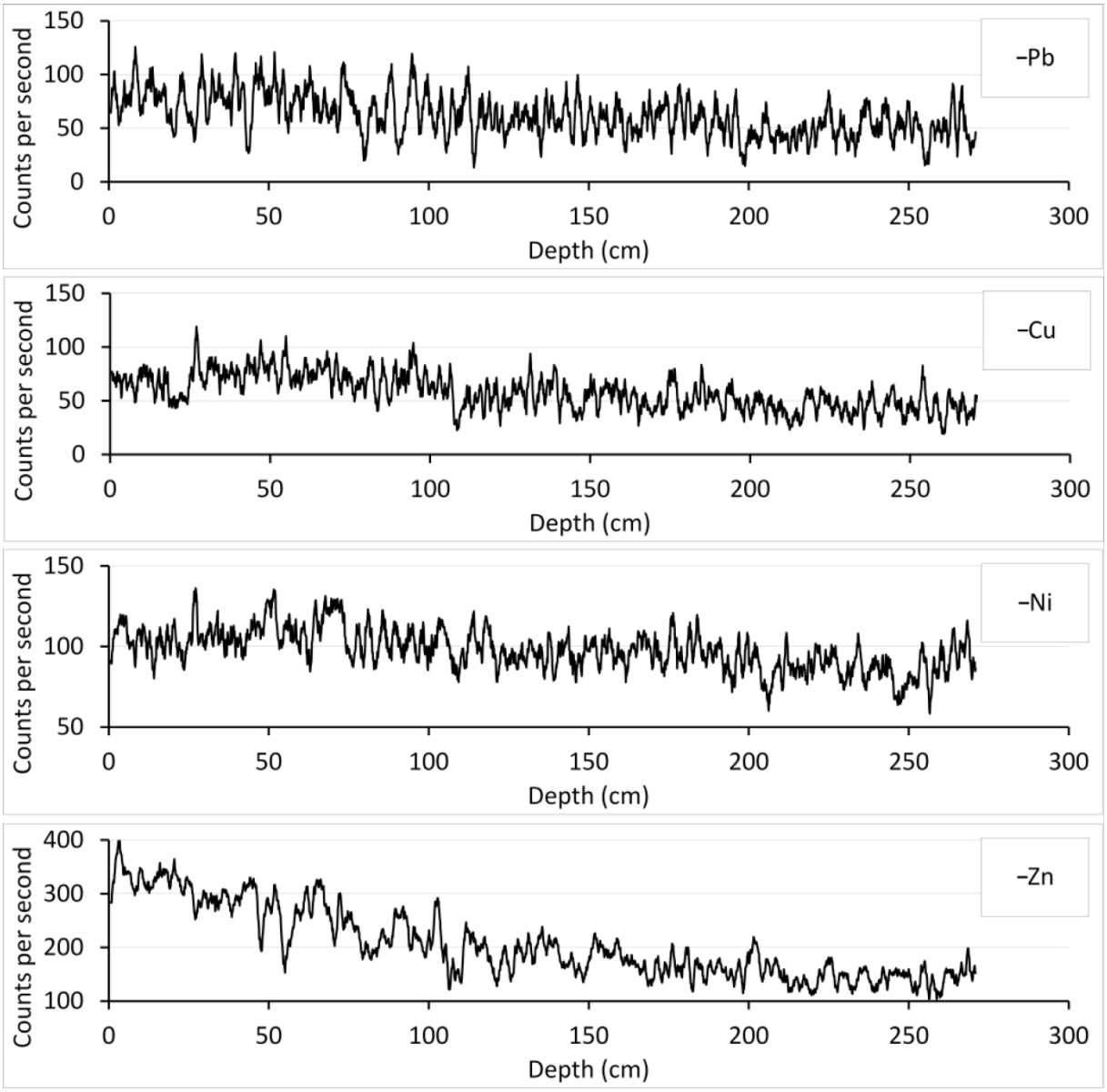

Figure A2 Karere 2 core: Zr/Rb ratio, Z-score, inferred floods, heavy metal geochemistry (Pb, Cu, Ni, Zn).

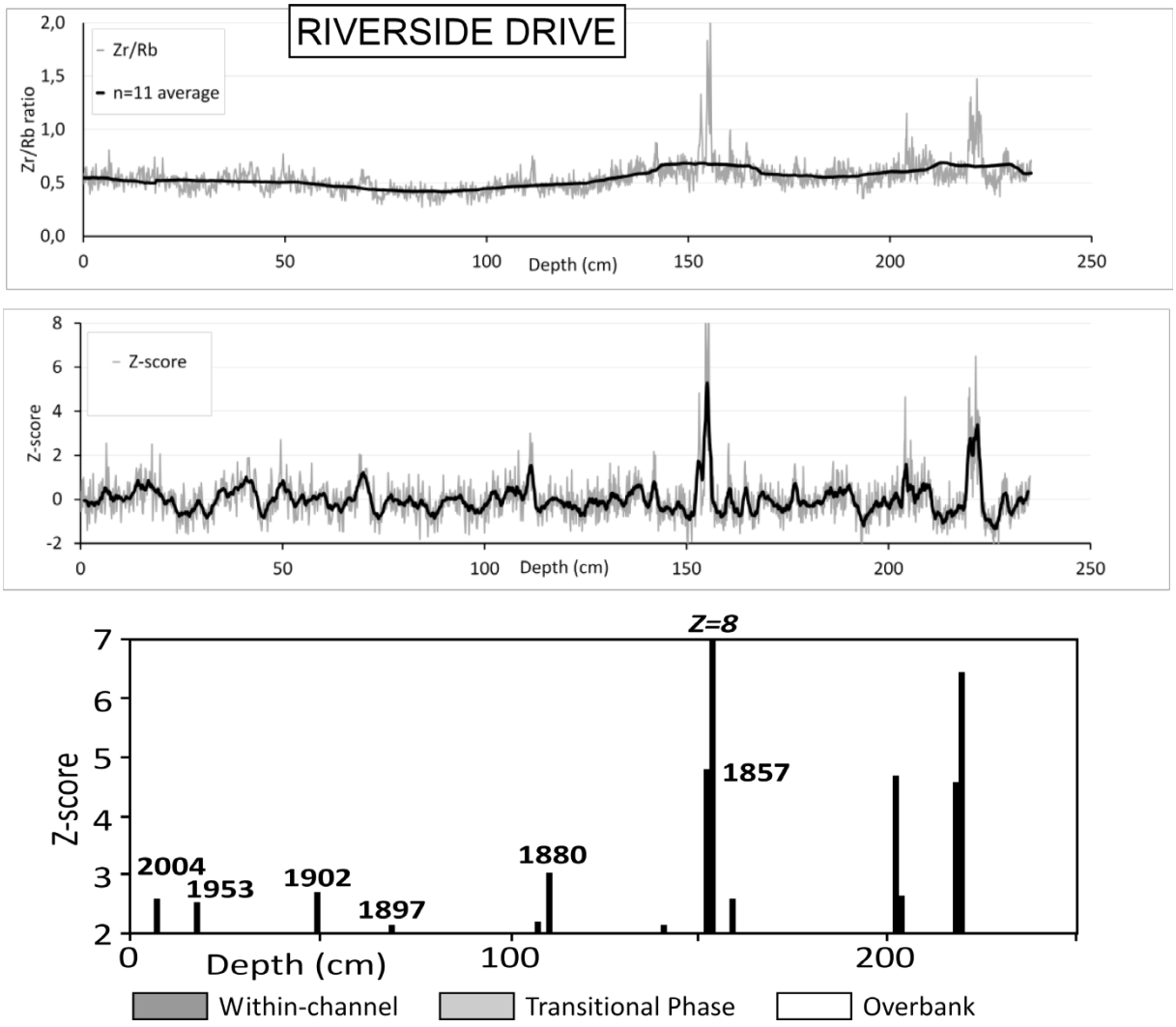
RIVERSIDE DRIVE
Zr/Rb
n=11 average
Zr/Rb ratio
2,0
1,5
1,0
0,5
0,0
0
50
100
150
200
250
Depth (cm)
Z-score
8
6
4
2
0
-2
Depth (cm)
Z=8
1857
1880
2004
1953
1902
1897
Z-score
7
6
5
4
3
2
0
100
200
Depth (cm)
Within-channel
Transitional Phase
Overbank

801

802

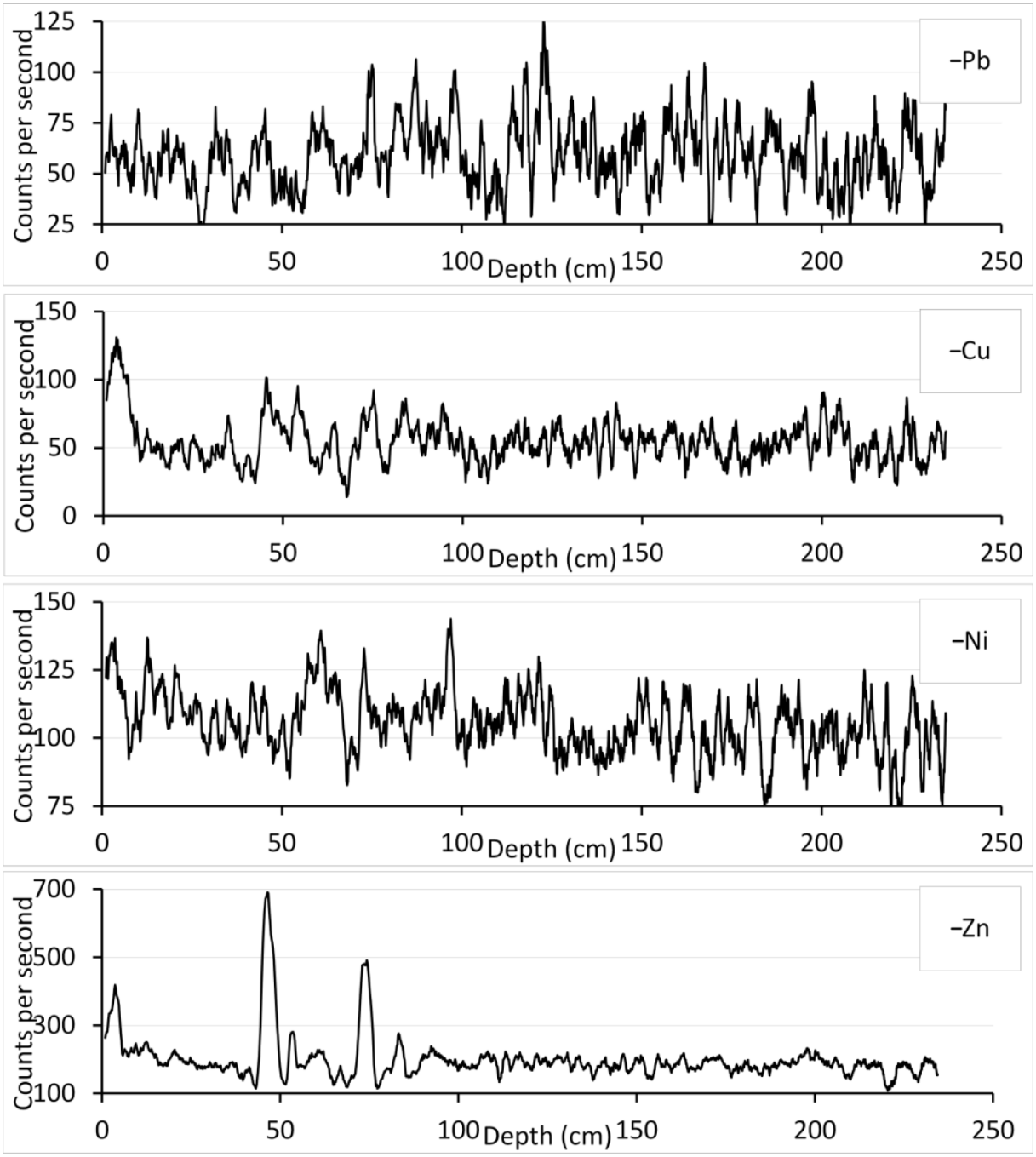

803

804 **Figure A3** Riverside Drive core: Zr/Rb ratio, Z-score, inferred floods, heavy metal geochemistry (Pb,
805 Cu, Ni, Zn)

806

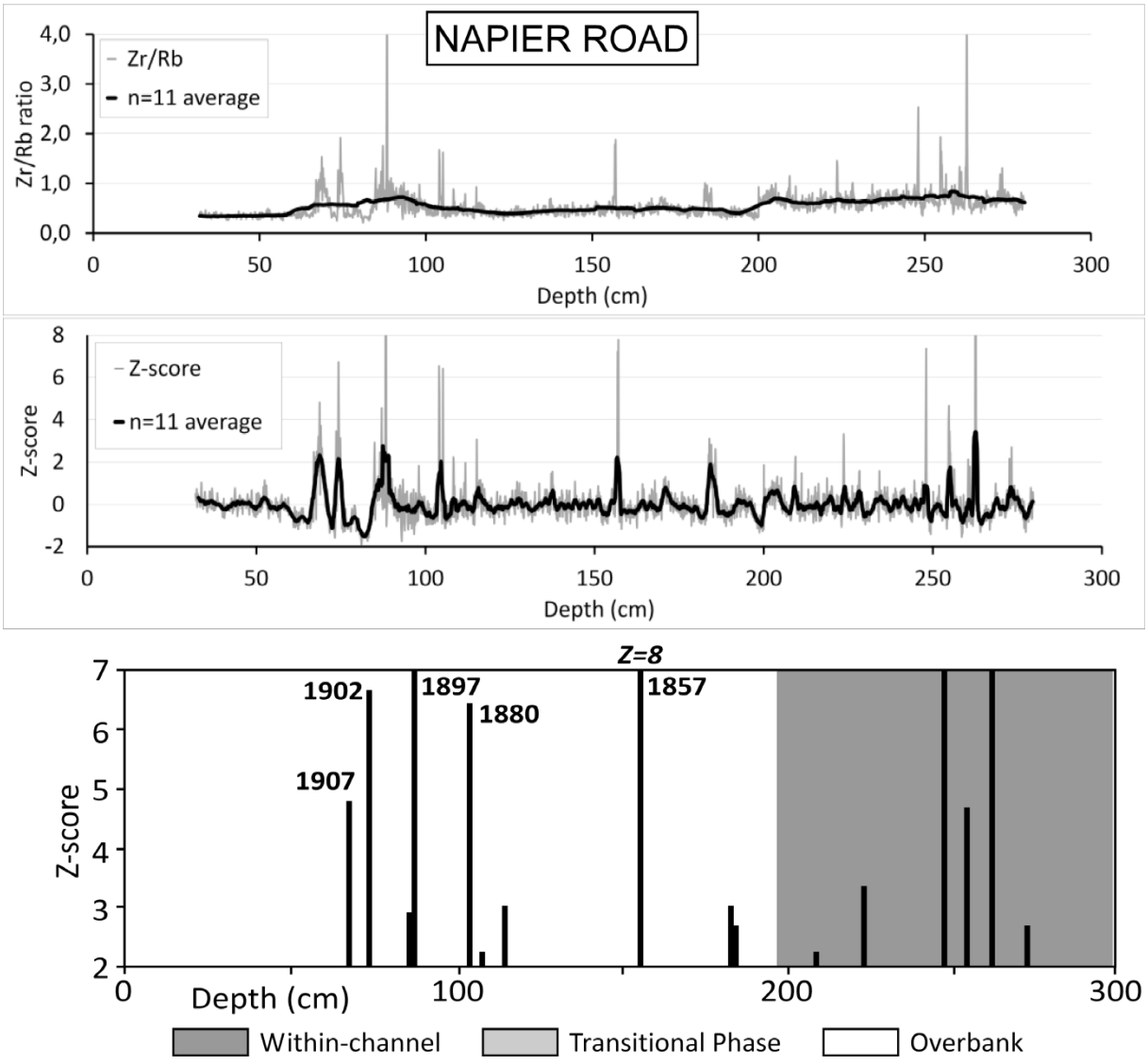
NAPIER ROAD
Zr/Rb
n=11 average
Zr/Rb ratio
4,0
3,0
2,0
1,0
0,0
0
50
100
150
200
250
300
Depth (cm)
Z-score
n=11 average
8
6
4
2
0
-2
Depth (cm)
Z=8
1902
1897
1880
1857
1907
7
6
5
4
3
2
Z-score
Depth (cm)
Within-channel
Transitional Phase
Overbank

807

808

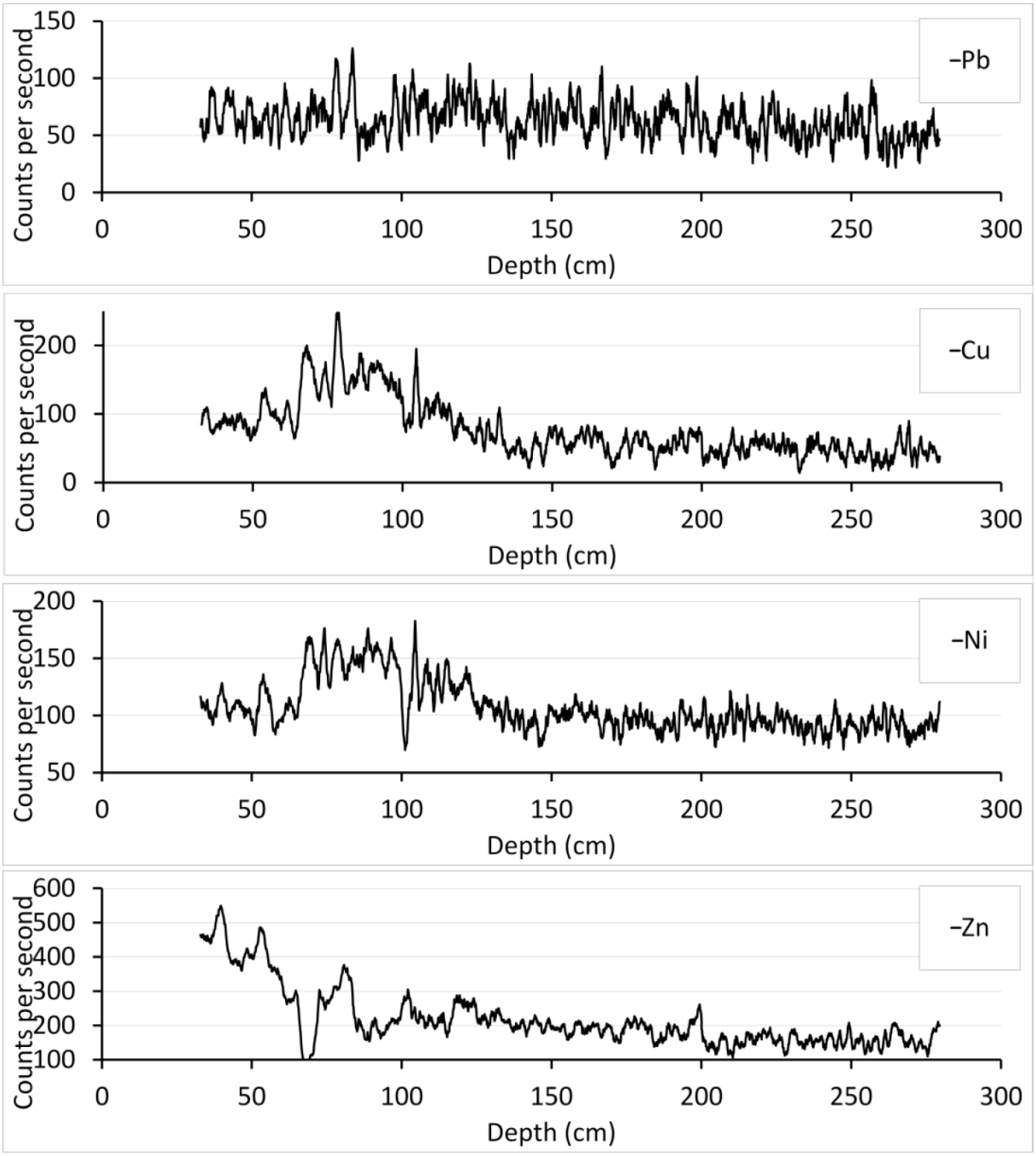

Figure A4 Napier Road core: Zr/Rb ratio, Z-score, inferred floods, heavy metal geochemistry (Pb, Cu, Ni, Zn)

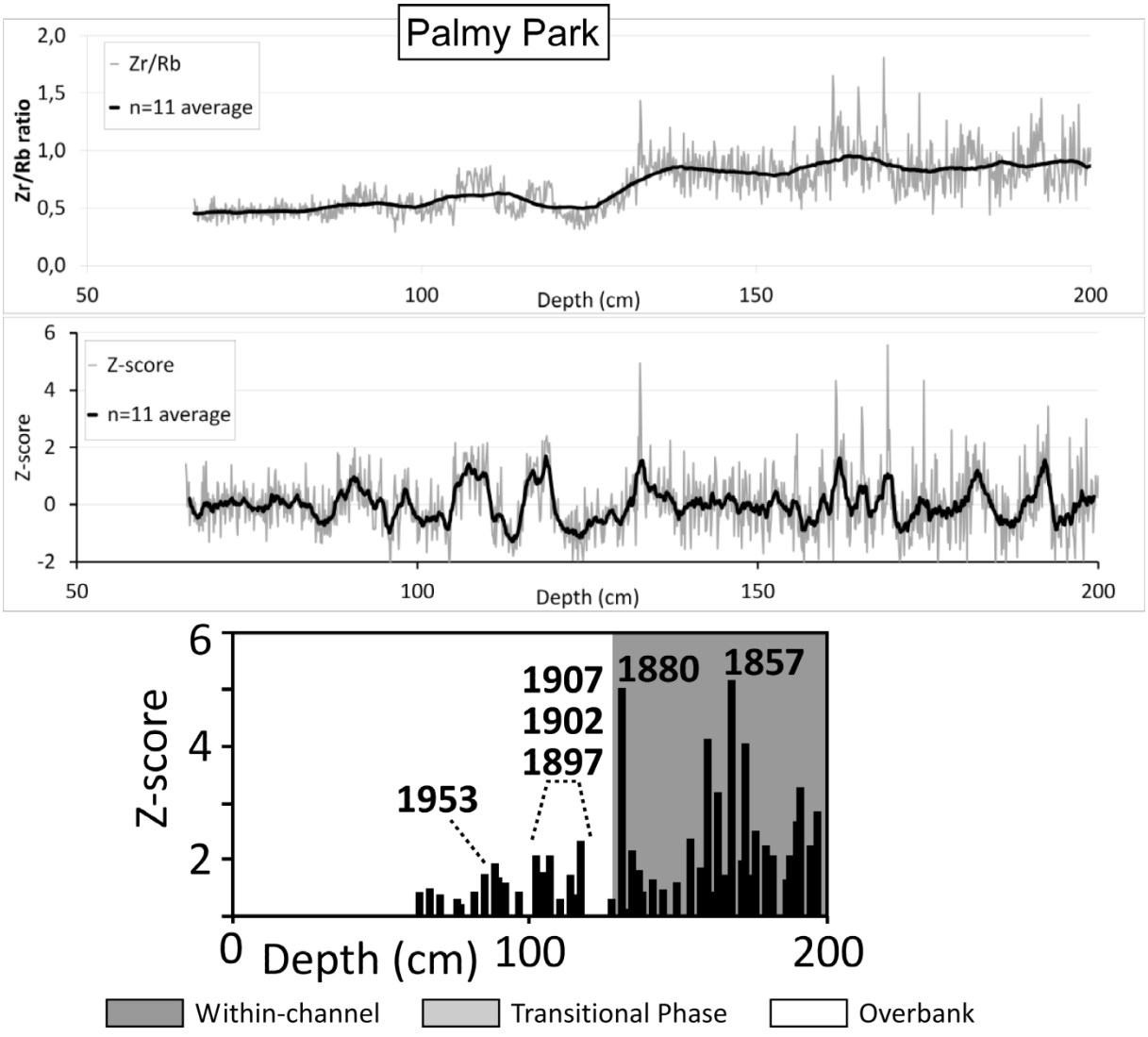
Palmy Park
Zr/Rb
n=11 average
Zr/Rb ratio
2,0
1,5
1,0
0,5
0,0
50
100
150
200
Depth (cm)
Z-score
n=11 average
6
4
2
0
-2
1907
1902
1897
1880
1857
1953
0
Within-channel
Transitional Phase
Overbank

813

814

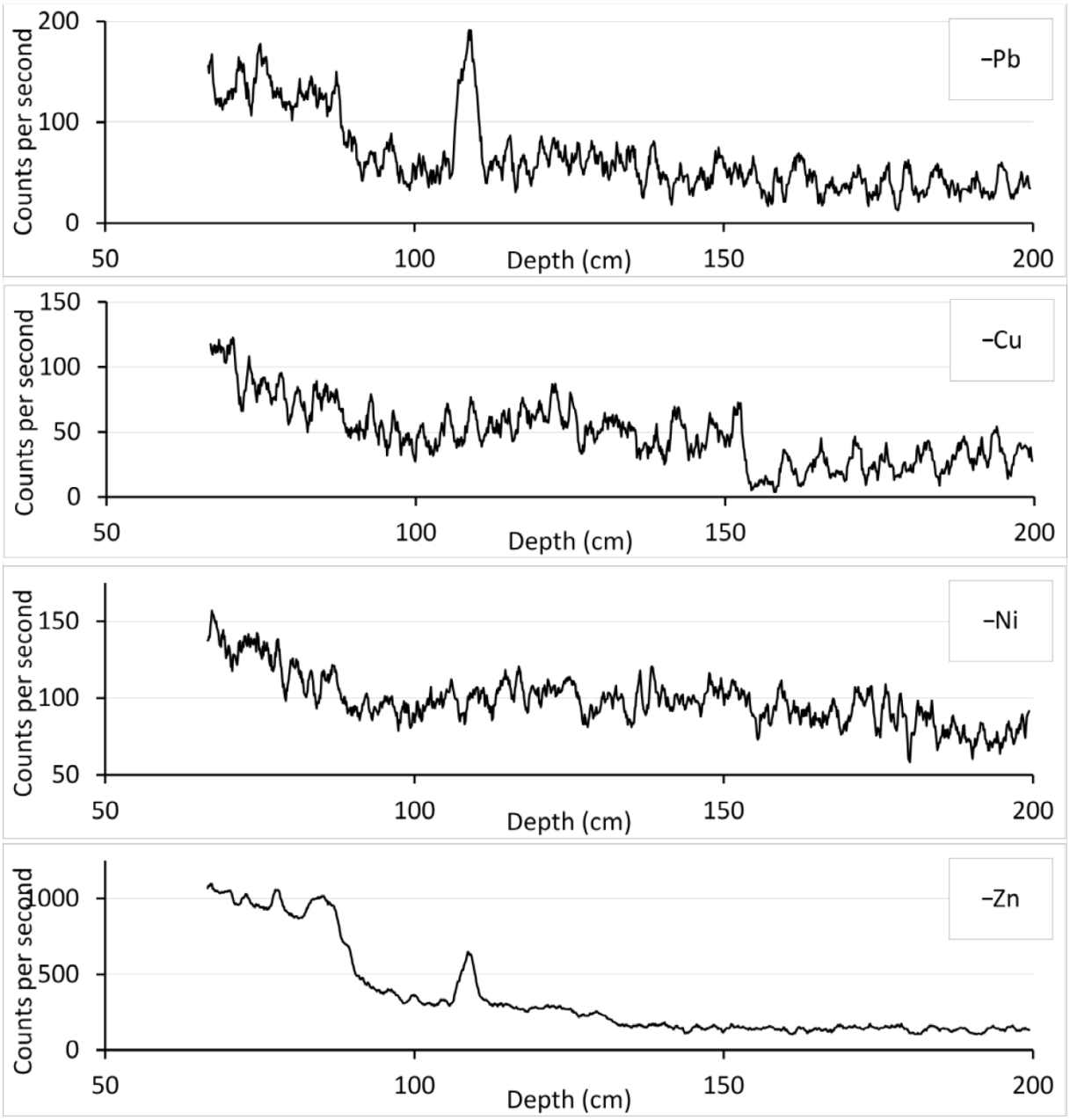

815

816 **Figure A5** Palmy Park core: Zr/Rb ratio, Z-score, inferred floods, heavy metal geochemistry (Pb, Cu,
817 Ni, Zn).

818

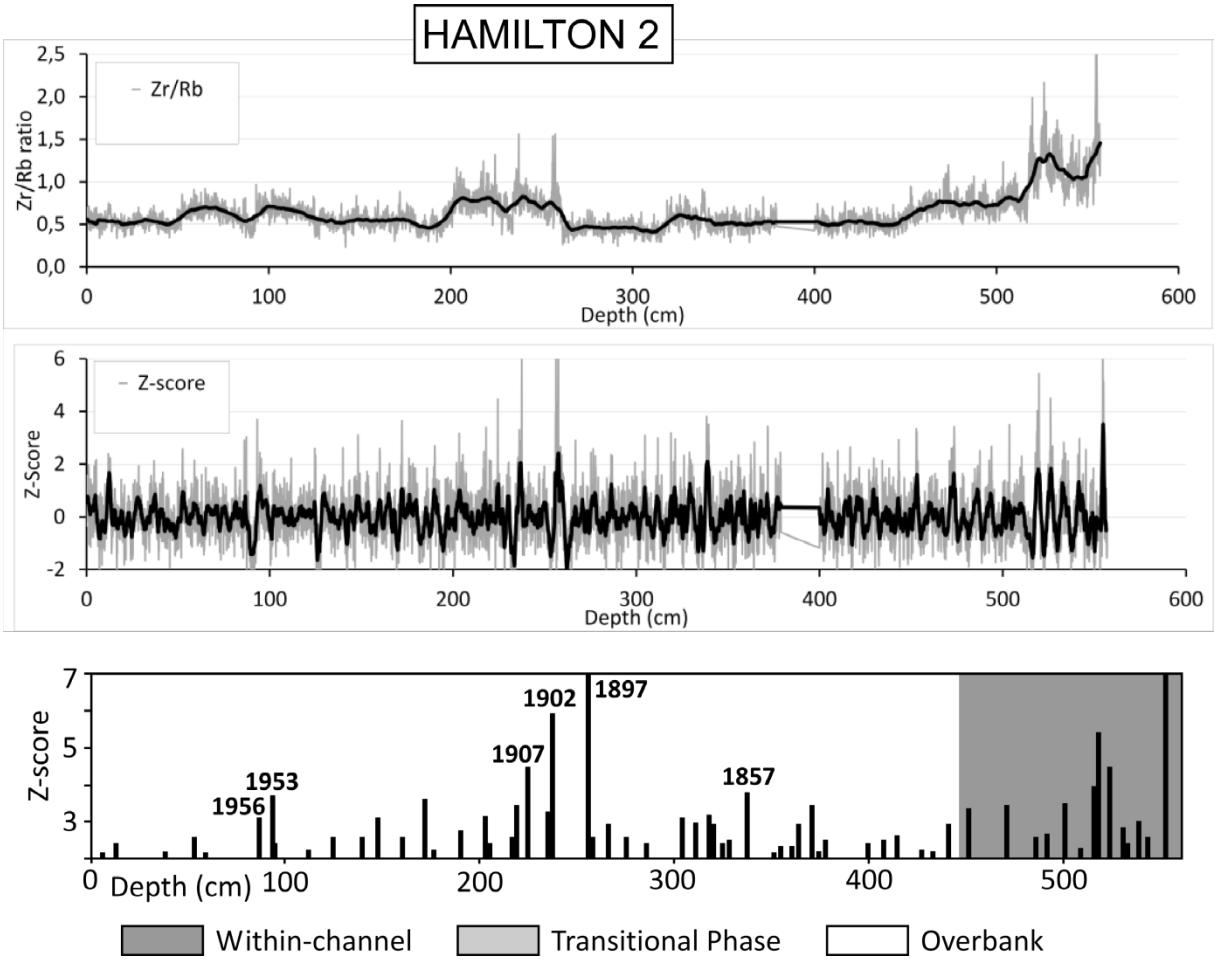
HAMILTON 2
Zr/Rb
Zr/Rb ratio
2,5
2,0
1,5
1,0
0,5
0,0
0
100
200
300
400
500
600
Depth (cm)
Z-score
Z-Score
6
4
2
0
-2
0
100
200
300
400
500
600
Depth (cm)
Z-score
7
5
3
1902
1897
1907
1953
1956
1857
0
Depth (cm)
100
200
300
400
500
Within-channel
Transitional Phase
Overbank

819

820

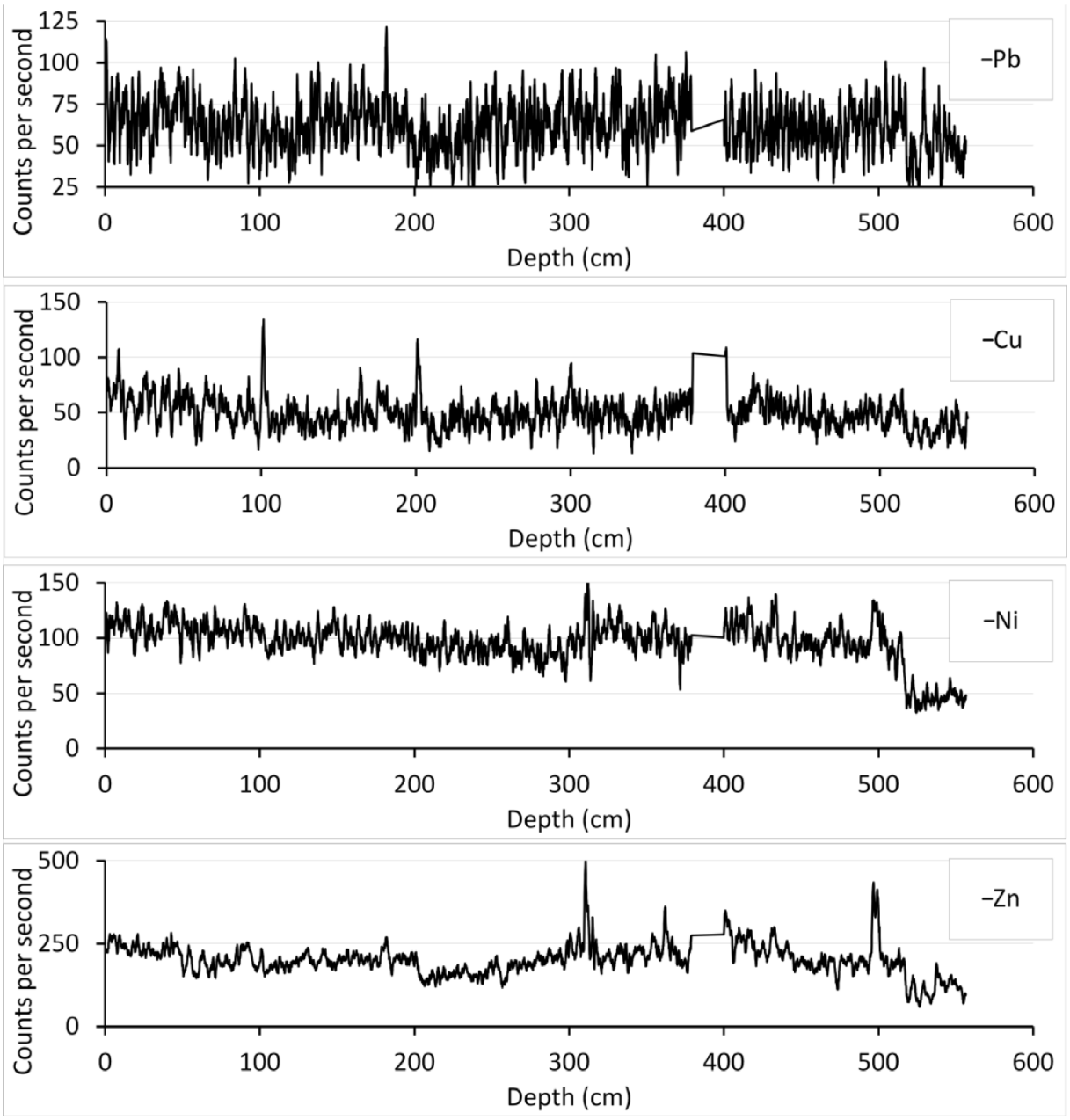

821

822 **Figure A6** Hamilton 2 core: Zr/Rb ratio, Z-score, inferred floods, heavy metal geochemistry (Pb, Cu,
823 Ni, Zn).

824

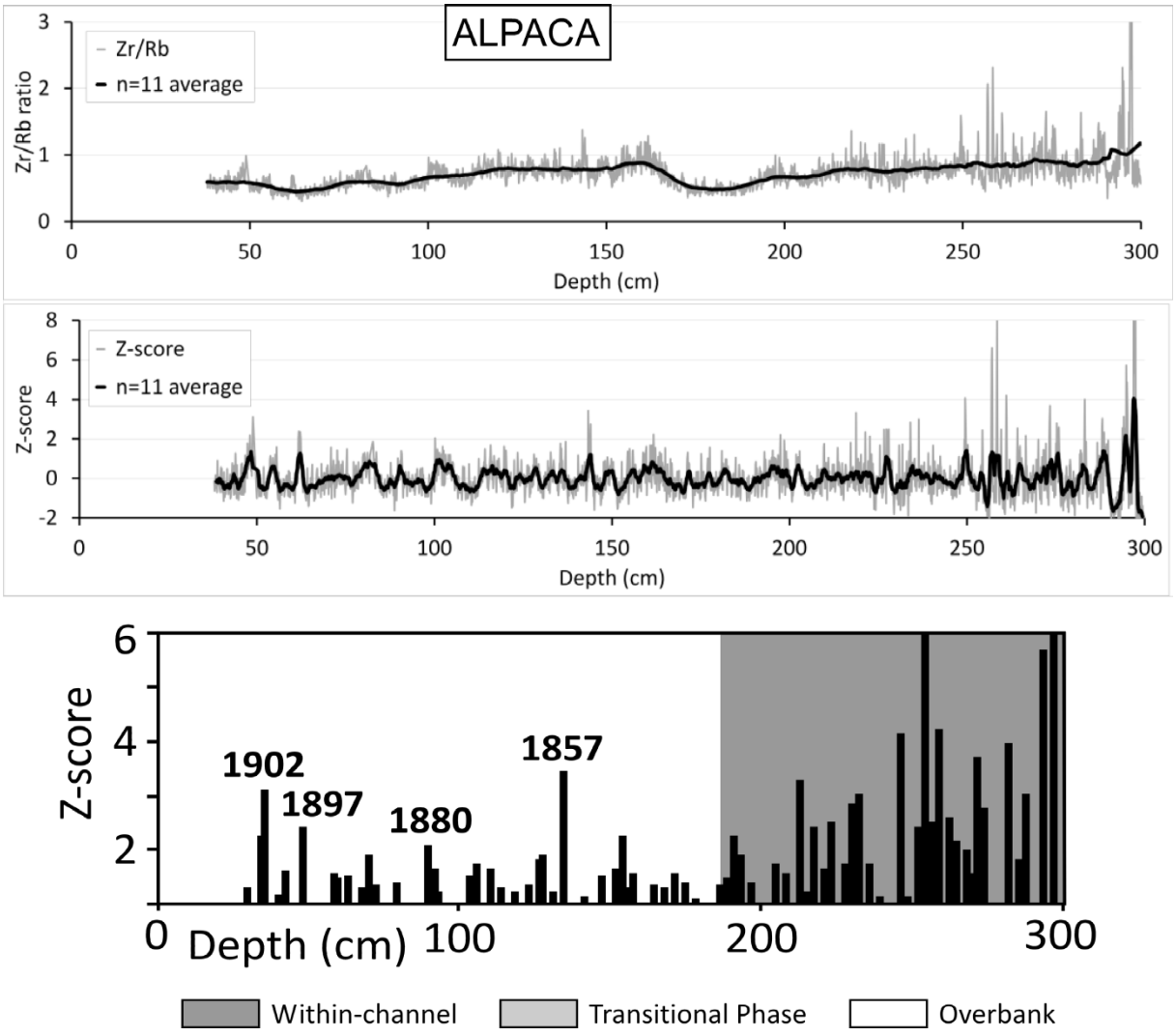
ALPACA
Zr/Rb
n=11 average
Zr/Rb ratio
Depth (cm)
Z-score
n=11 average
Z-score
Depth (cm)
Z-score
1902
1897
1880
1857
Depth (cm)
Within-channel
Transitional Phase
Overbank

825

826

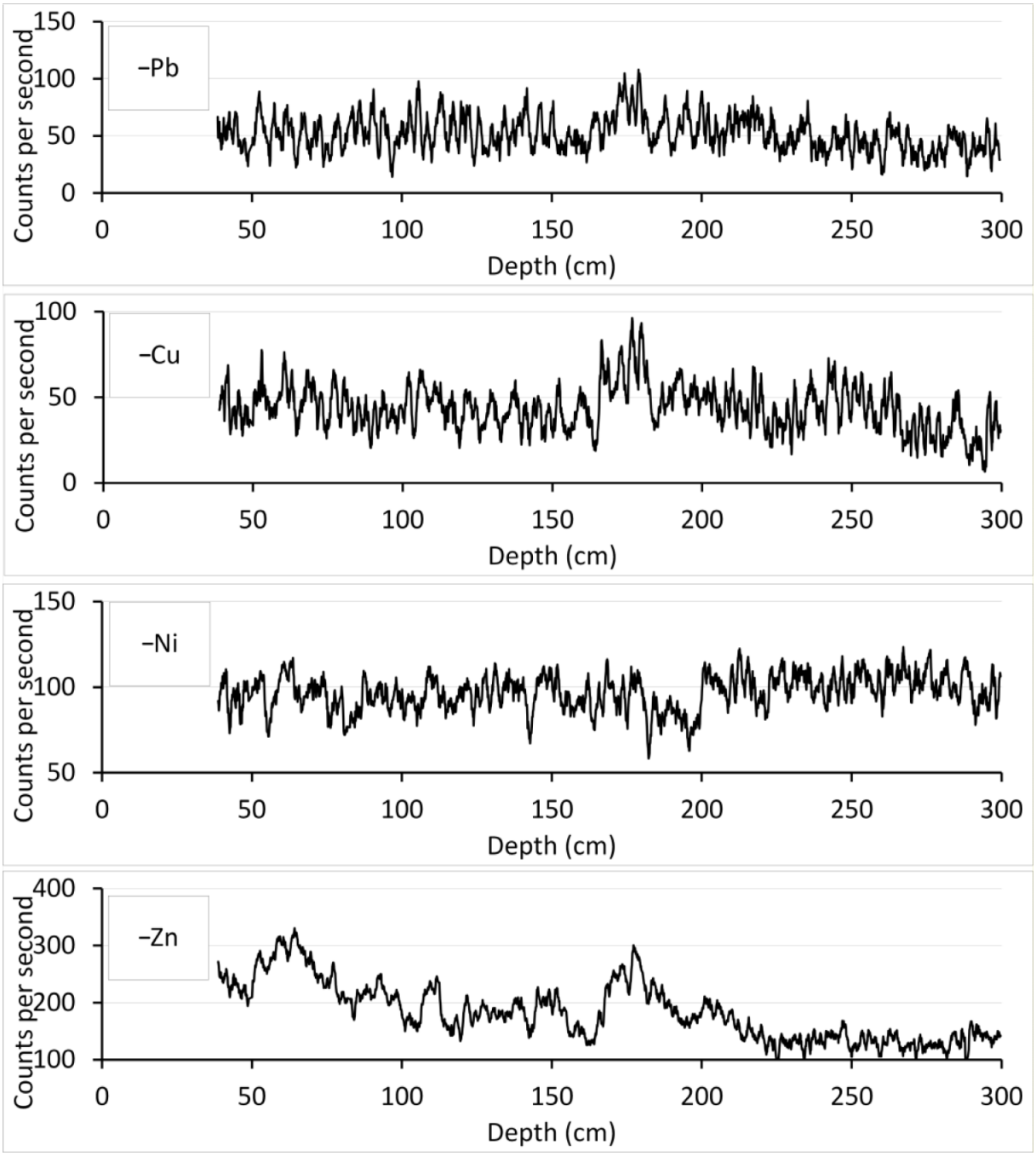

827

828 **Figure A7** Alpaca core: Zr/Rb ratio, Z-score, inferred floods, heavy metal geochemistry (Pb, Cu, Ni,
829 Zn).

830

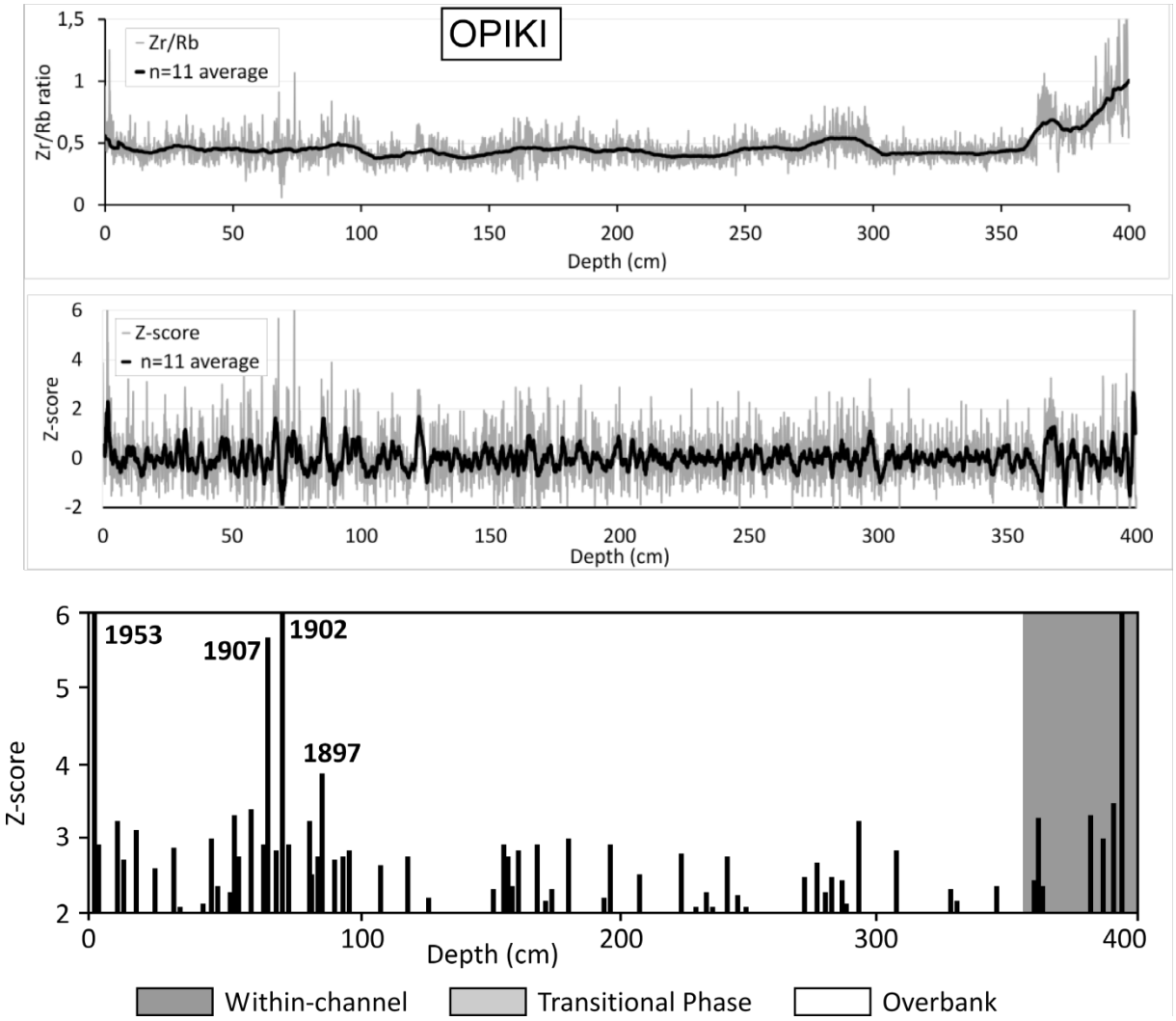
OPIKI
Zr/Rb
n=11 average
Zr/Rb ratio
Depth (cm)
Z-score
n=11 average
Z-score
Depth (cm)
1953
1907
1902
1897
Z-score
Depth (cm)
Within-channel
Transitional Phase
Overbank

831

832

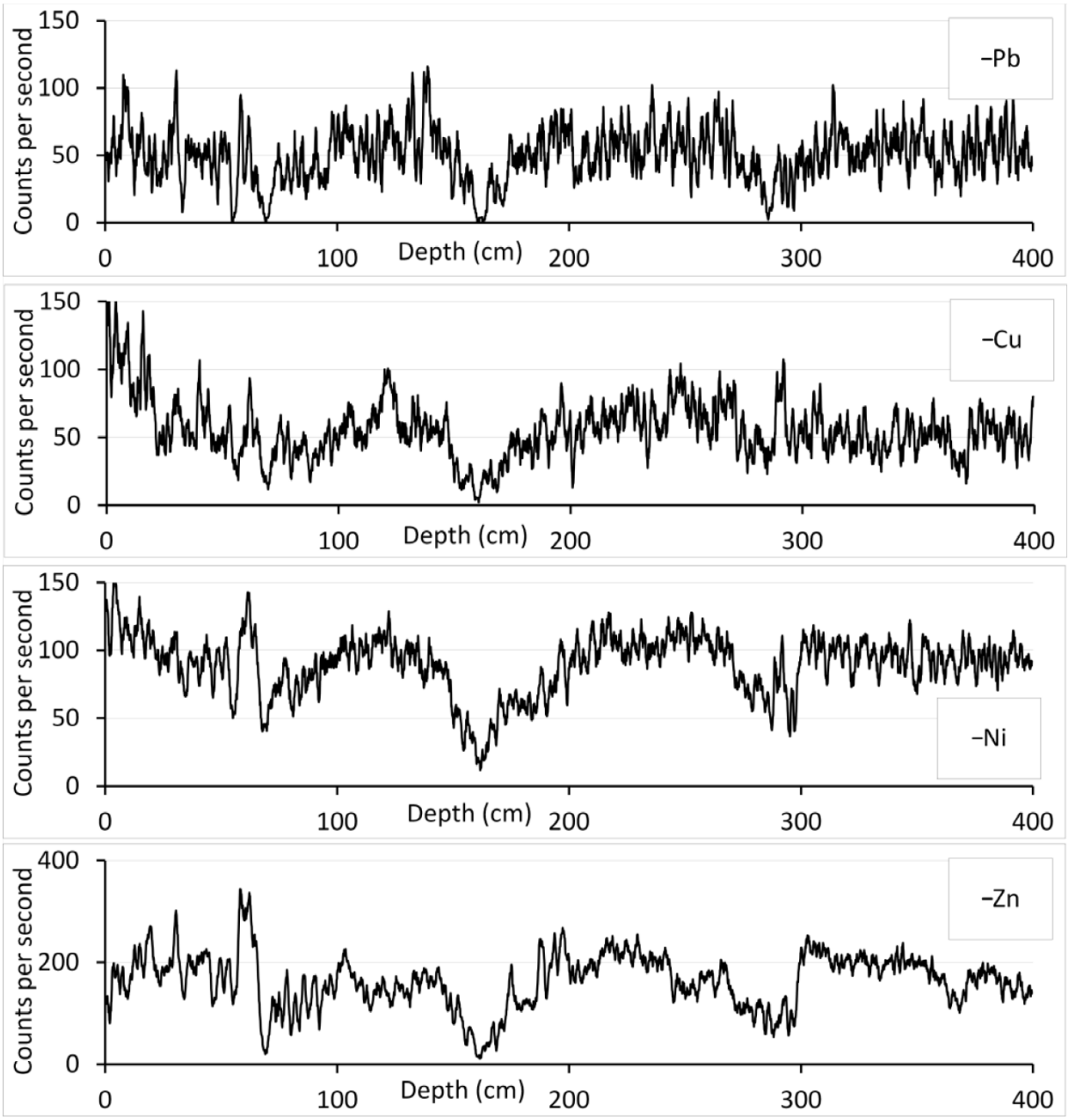

Figure A8 Opiki core: Zr/Rb ratio, Z-score, inferred floods, heavy metal geochemistry (Pb, Cu, Ni, Zn).

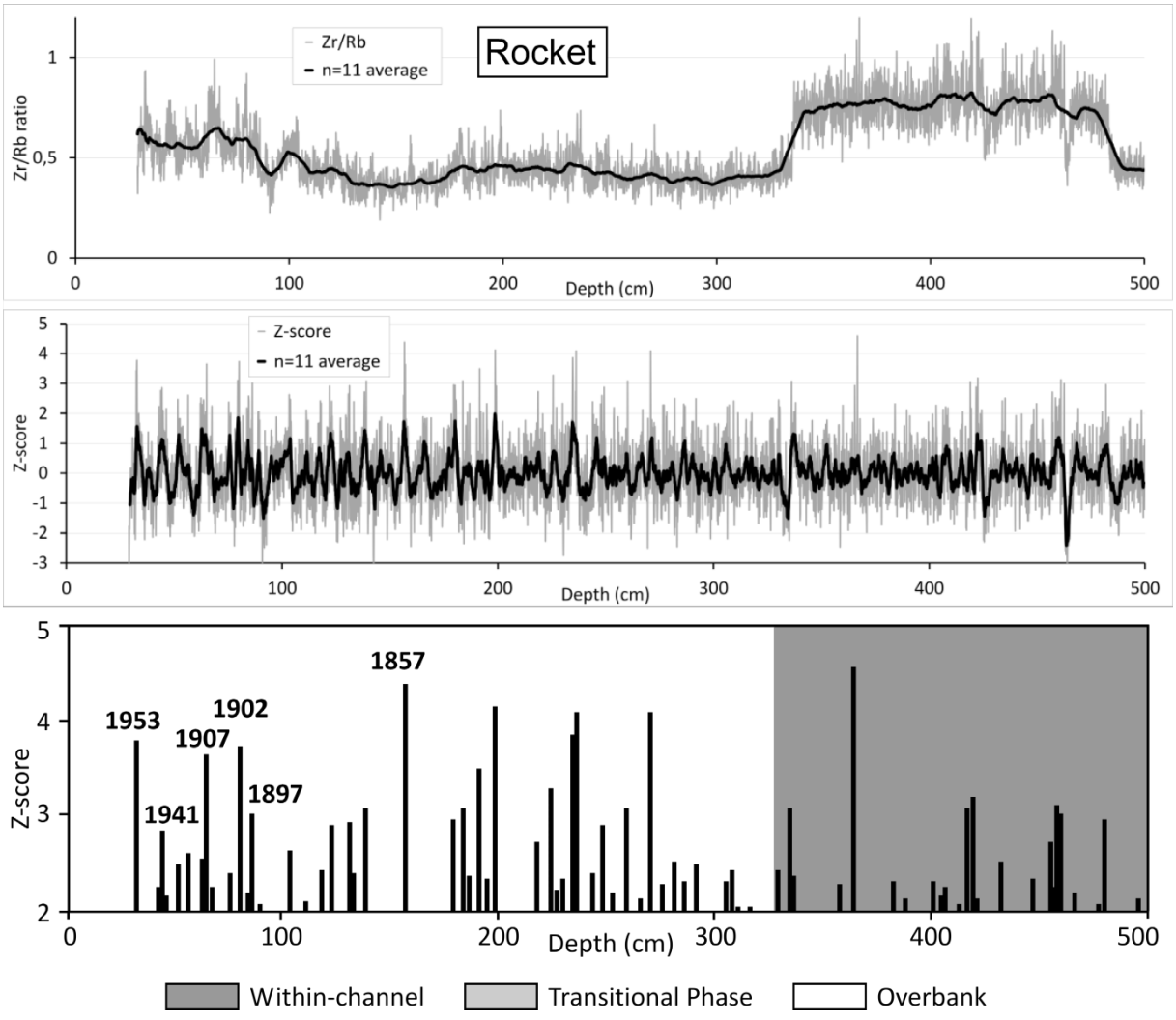
Rocket
Zr/Rb
n=11 average
Zr/Rb ratio
Depth (cm)
Z-score
n=11 average
Z-score
Depth (cm)
1857
1953
1902
1907
1897
1941
Z-score
Depth (cm)
Within-channel
Transitional Phase
Overbank

836

837

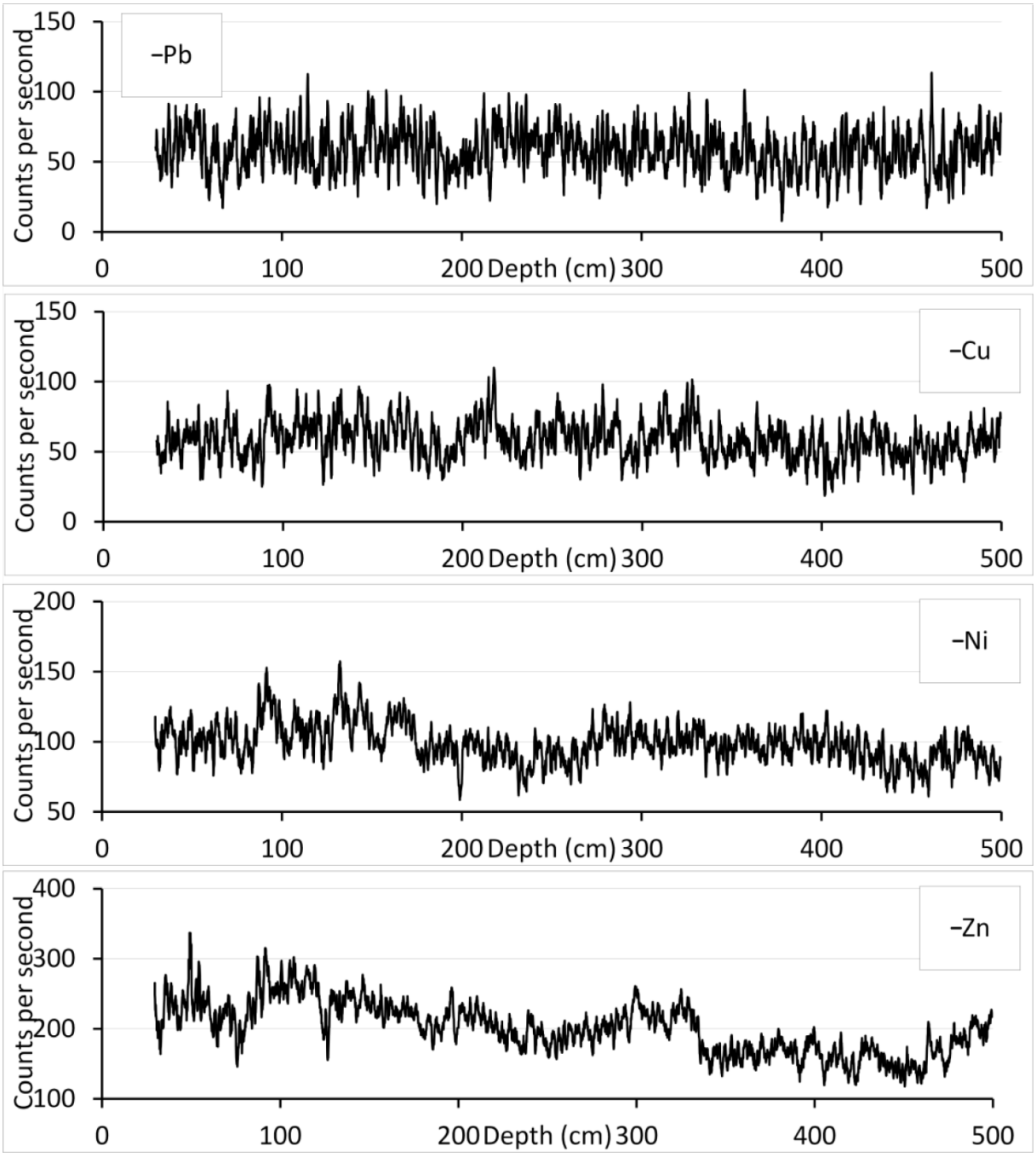

838

839 **Figure A9** Rocket core: Zr/Rb ratio, Z-score, inferred floods, heavy metal geochemistry (Pb, Cu, Ni,
840 Zn).

841